Experimental investigations on the influence of the system properties and the drop diameter on drop breakage

Studienarbeit

Daniel Zedel

Matrikelnummer: 210455

26. Oktober 2010

Technische Universität Berlin
Fakultät 3: Prozesswissenschaften
Fachgebiet Verfahrenstechnik

Betreuer: Prof. Dr.-Ing. M. Kraume
Dipl.-Ing. S. Hermann

Technische Universität Berlin

Thesis declaration

I hereby declare, that the student research project: *Experimental investigations on the influence of the system properties and the drop diameter on drop breakage* is my own, unaided work and that all sources of information and references being used are listed to the best of my knowledge.

Die selbständige und eigenhändige Ausfertigung der Studienarbeit: *Experimentelle Untersuchungen zum Einfluss des Stoffsystems und der Tropfengröße auf den Tropfenbruch* versichere ich an Eides statt.

Berlin, den 26. Oktober 2010

_____

(Daniel Zedel)

Abstract

In this work, the influence of the system properties on single drop breakage events was analysed separated from coalescence in a drop breakage cell. The breakage probability and breakage rate, as well as the initial number of daughter drops and the breakage location, have been studied using high speed imaging. The influence of the framerate on the recognition of binary breakage was studied in order to find out if tertiary and higher breakages exist or if they are an effect of a not sufficiant framerate. Drop generation as a function of the system properties and the means of drop creation was investigated in order to produce small droplets ($200 - 500$ µm). Also theoretical and experimental preexaminations were conducted with the aim to improve the existing set-up and to make research on small drops accessable.

It was quantitatively measured that more stable drops have decreased breakage rates and that the number of initial daughter drops decreases with increasing framerate, meaning that the fraction of binary breakage increases. The number of initial daughter drops also depends on the system properties. Drops that are more stable tend more towards binary breakage. It was possible to generate drops with a diameter lower than before by varying the position of drop generation, as well as the equipment used (needles). New insights on possible improvements of the current set-up concerning drop generation and breakage experiments could be gained.

Zusammenfassung

In dieser Arbeit wurde der Einfluss des Stoffsystems auf den Tropfenbruch von Einzeltropfen in einem speziell entwickelten Zerfallskanal untersucht. Die Bruchwahrscheinlichkeit und die Bruchzeit, sowie die Anzahl der Tochtertropfen nach dem ersten Bruch und der Bruchort, wurden mithilfe von Hochgeschwindigkeitsaufnahmen ausgewertet. Der Einfluss der Bildaufnahmefrequenz auf die Brucherkennung wurde ebenfalls untersucht. Es galt heraus zu finden ob tertiäre oder höhere Brüche existieren, oder ob diese ein Effekt der nicht ausreichenden Aufnahmefrequenz sind. Außerdem wurde die Tropfenerzeugung in Abhängigkeit des Stoffsystems und der Art der Erzeugung analysiert, mit dem Ziel, kleine Tropfen ($200 - 500$ µm) zu erzeugen. Theoretische und experimentelle Voruntersuchungen wurden mit dem Ziel durchgeführt, den aktuellen Versuchsaufbau zu verbessern und ihn für die Auflösung kleiner Tropfen zugänglich zu machen.

Es wurde quantitativ bestimmt, dass stabilere Tropfen eine verringerte Bruchrate aufweisen und dass die Anzahl der Tochtertropfen nach dem ersten Bruch bei steigender Bildaufnahmefrequenz sinkt, was bedeutet, dass der Anteil der binären Brüche zunimmt. Es besteht ebenfalls eine Abhängigkeit der Tochtertropfenanzahl vom Stoffsystem. Stabilere Tropfen tendieren eher dazu binär zu brechen. Es war möglich mit dem experimentellen Aufbau, durch Variation des Ortes der Tropfenerzeugung und der Ausstattung (Nadeln), Tropfen mit kleinerem Durchmesser zu erzeugen. Ebenfalls konnten neue Einsichten in die Verbesserung des aktuellen Versuchsaufbaus gewonnen werden, sei es bei der Tropfenerzeugung, oder bei den Bruchexperimenten.

Contents

Nomenclature

Roman letters

$\dot{A}$	Leaving flux term in balance equation	[*variable*]
A	Area	[m^2]
C	Constants	[*variable*]
D	Sink term	[−]
d	Diameter	[m]
E	Surface energy	[J]
G	Source term	[−]
g	Breakage rate	[1 /s]
l	Inner coordinate	[−]
N	Number, amount	[−]
n	Number distribution	[−]
$\dot{S}$	Storage term in balance equation	[*variable*]
t	Time	[s]
$\dot{V}$	Flowrate	[m^3/s]
V	Volume	[m^3]
v	Velocity	[m/s]
$\dot{W}$	Source/sink term in balance equation	[*variable*]
x, y	Spatial coordinate	[m]
fps	Frames per second	[1 /s]
$\dot{Z}$	Incoming flux term in balance equation	[*variable*]

Greek symbols

α	Damping factor	[−]
β	Daughter drop size distribution	[1 /m]
η	Dynamic viscosity	[kg/(m s)]
ε	Energy dissipation rate	[m^2/s^3]
γ	Interfacial tension	[N/m]
ρ	Density	[kg/m^3]
σ	Standard deviation	[*variable*]
τ	Stress	[N/m^2]

Indices

$\bar{}$	Arithmatic mean value
b	Value at the bottom entry point
$break$	Breakage
c	Continuous phase
$coal$	Coalescence
$crit$	Critical value
d	Dispersed phase
m	Value at the middle entry point
max	Maximum value
p	Particle
t	Value at the top entry point
tot	Total

1 Introduction

1.1 Motivation

There are numerous applications in industry, where reactions and mass-, as well as energy-transfer between two immiscible fluids are the major concerns. In most cases it is necessary to increase the contact area between the two phases in order to achieve practicable product- or energy-streams, or to reduce the time it takes a process to complete. Though when considering the reduction of the settling time, bigger drops are desired. It usually is a multi-level-optimization with the goal of achieving the best product quality with the lowest power consumption and the lowest negative impact on the environment.

When trying to increase the contact area one has to focus on drop sizes and the underlying principles that lead to the formation of drops in immiscible liquid-liquid dispersions, for example in stirred vessels or static mixers, in the first place. It was found that drop breakage and coalescence determine the drop size distributions and in order to predict that distribution both phenomena have to be understood.

The exact modelling of drop breakage and coalescence processes is the most important factor to make expensive and time consuming experiments superficial. Scientific research, reviewed in Liao and Lucas (2009, 2010), identified a multitude of descriptions of drop breakage and coalescence.

While in the stirred tank both, drop breakage and coalescence influence the drop size distribution, drop breakage can be studied in the absence of coalescence. One approach is hindering the coalescence in s stirred tank by using dilute systems or by adding a surfactant. In this work another possibility is used: an especially built single drop breakage cell were the breakage of single drops can be investigated. This has the advantage of a deeper understanding of one phenomenon at a time. Both methods, observations in a stirred tank and in a single drop breakage cell are described in Gäbler et al. (2005). The method preferred here is to isolate drop breakage and to identify its influencing factors experimentally.

Drop sizes, as seen in practical applications, have not yet been fully investigated. The main focus with the single drop breakage cell used in this work, lay on drop sizes larger than 0.66 mm (Zillmer, 2010), which, while easy to create, are in the upper range of drops found in industry vessels (Paul et al., 2004).

Therefore one aim of this project was to to establish a way to create drop sizes considerably smaller than before, but also to be able to compare the results with previous research. Another aim was to investigate the influence of the system properties on the drop breakage process.

1.2 Structure

In the following second section a theoretical foundation will be laid out, including a description of fluid particle breakup in general, as well as the introduction of drop size distributions and its possible description by using the Population Balance Equation (PBE). An overview of some theoretical models for the breakage rate and the number of initial daughter drops will be given and a brief outline of possible experimental procedures used by other researchers to investigate drop breakage.

The third section will deal with the experimental set-up and procedures used in this work, giving an outline of all the steps involved. Also the system properties of the dispersed phase and a short summary of the image processing will be included therein.

The theoretical considerations concerning the drop generation and the analysis of the breakage events will be laid out in the following section, describing ways of creating small drops and increasing the image resolution.

Section five will show the experimental results of the influence of the system properties which will then be explained and discussed. Furthermore the results of the preparation of creating small drops will be displayed.

In the final section a general summary is be given and possibilities for further work in this field will be pointed out.

2 Theoretical background

According to Alopaeus et al. (1999) there are different phenomena that influence drop size distributions in two-phase processes in a stirred vessel. Three main aspects are identified and described further:

Breakage and coalescence of droplets: This is affected by local mechanical conditions like turbulent energy dissipation and shear forces; and also by physical properties like the viscosity and density of the phases. Interfacial tension and other interfacial phenomena like the surface charge of the particles plays a role as well, as it may, for example, hinder coalescence.

Growth and nucleation of droplets: Due to mass transfer into or out of the particles their size is influenced. It also can come to droplet growth or shrinkage as a result of chemical reactions that do not conserve volume. New drops may also be generated through nucleation when the system becomes thermodynamically unstable.

Feed or discharge of droplets in a particular region: When it comes to relative velocities between the continuous and the dispersed phase, it can occur that the drop size distribution is altered in the affected regions.

In this work the focus is laid on breakage and coalescence of droplets, more precisely only on drop breakage.

2.1 Fluid particle breakup in general

According to the literature review of theoretical models for drop and bubble breakup in turbulent dispersions by Liao and Lucas (2009), there are several mechanisms that can influence fluid particle breakup.

Continuous phase hydrodynamics and interfacial interactions play a major role in the processes of drop breakage. There are external forces and stresses which try to break up the particle, exerted on it by the continuous phase, and there are the internal forces and stresses which try to hold the particle together. Those stresses are in balance as long as the particle exists as a whole and by knowing the terms of the balance one can predict a maximum stable drop diameter, that depends on the hydrodynamic conditions in the liquid surrounding the particle and on the characteristics of the dispersed phase as well.

Liao and Lucas distinguished four main categories of breakage mechanisms. The classification is as follows:

A) Turbulent fluctuations and drop-eddy collisions
B) Viscous shear stress
C) Shearing-off process
D) Interfacial instability

Turbulent fluctuations and drop-eddy collisions: Breakup mainly occurs through turbulent pressure fluctuations along the drops' surface, or by drop-eddy collisions. In both cases the spherical shape of the drop can be modified to such an extent that the drop becomes unstable. The two main stresses involved are, on the external side, the dynamic pressure difference $\tau_{pressure}$ around the particle and, on the internal side, its surface stress $\tau_{surface}$. Viscous stresses inside the particle usually are neglected. So the breakage depends on the force balance of those two stresses and one can determine if a particle will break when one examines the extent of the deformation. A dimensionless number can be generated by considering the two stresses mentioned above, the Weber number: $We = \tau_{pressure}/\tau_{surface}$. When the Weber number increases, so does the deformation of the particle. As soon as a critical value is reached, the particle breaks.

There are various criteria for breakup, defined by each author reviewed by Liao and Lucas (2009). Some of them are:

- turbulent kinetic energy of the particle (or of the hitting eddy) is greater than a critical value (Coulaloglou and Tavlarides, 1977),
- velocity fluctuations around the surface of the particle are greater than a critical value (Alopaeus et al., 2002), and
- turbulent kinetic energy of the bombarding eddies is greater than a critical energy value (Martínez-Bazán et al., 1999).

A more detailed description of those models will be given in Section 2.3.1.

Viscous shear stress: Here breakup is caused by viscous shear forces in the continuous phase, inducing a velocity gradient around the interface of the drop and deforming it. If a trailing drop has its larger part ouside a wake region, shear stresses appear due to a wake effect and the drop may be caused to split by the shear stress across the wake boundary. This is a result of elongation, surface indentation and necking. Particles are firstly elongated into two almost equal sized lumps seperated by a thread and they break into two equal sized daughters and a series of smaller particles (satellites) that correspond to the thread between the lumps. Elongation into a cylindrical thread is also possible, which leads to even smaller droplets.

Shearing-off process: When considering particles of larger size, the breakup mechanisms get more complicated due to shearing-off and interfacial instability, both of which result from

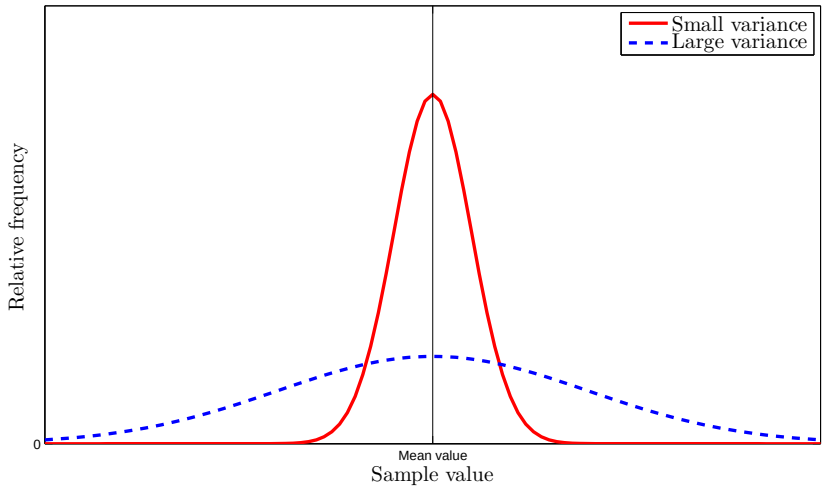

Figure 2.1: Generic density functions

a velocity difference across the interface. One characteristic is called erosive breakage, where a number of small particles is being sheared-off from a large one.

Interfacial instability: All the above mentioned mechanisms depend on the flow characteristics in the continuous phase. Even in the absence of a net flow of the continuous phase, breakup can be caused by interfacial instabilities, as is the case when considering rising bubbles or falling drops in liquid.

2.2 Drop size distribution and Population Balance Equation

To describe the state of a two-phase system consisting of a continuous and a dispersed phase the drop size distribution of the dispersed phase is used. Some generic example distributions are given in Figure 2.1 and the corresponding cumulative distributions in Figure 2.2. The distributions are characterized by a mean value and a variance. The variance describes an average distance value of the variable from its mean value.

One (Small variance) shows a narrow distribution while the other (Large variance) shows a wide one. This means that in the first case almost all the events are in a narrow region around the mean value. In the second case the events are varying widely. In the cumulative distributions one can also distinguished between a narrow and a wide variation around the mean value.

When drops undergo changes due to breakup, coalescence, growth and nucleation or feed and discharge, the drop size distribution changes. These changes can be mathematically described with the use of the Population Balance Equation. It considers fluid particles of a certain characteristic entering and leaving a control volume by different mechanisms, for example convection,

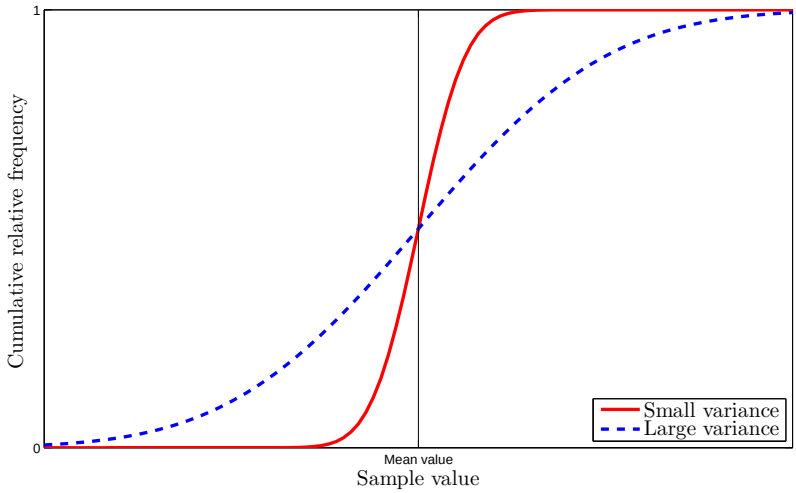

Figure 2.2: Generic cumulative distribution functions

growth or shrinkage and breakup or coalescence.

The main idea is to write a global balance of all those factors and in the end get a drop size distribution, corresponding to the influence of each and every factor. According to Paschedag (2004) one has to consider the inner and outer coordinates of the particle, that means that, additional to the spatial coordinates, to energy, mass and impulse (outer coordinates) the inner coordinates (i.e. diameter of the particle or its mass, l in general) have to be taken into account and an interval (control volume) has to be defined.

The concept of the global balance equation is used for the diameter: the storage of the balanced quantity ($\dot{S}$) in a volume has to be equal to the sum of the fluxes of this quantity through the boundaries ($\dot{Z} - \dot{A}$) and the volumetric sources/sinks ($\dot{W}$).

$$\dot{S} = \dot{Z} - \dot{A} \pm \dot{W} \tag{2.1}$$

Only breakage and coalescence will be considered from now on, so particle growth or shrinkage, as well as feed or discharge will be neglected. All those factors can be classified as parts of the balance equation. For example feed and discharge can be represented by the fluxes through the boundaries and breakage and coalescence are considered to be volumetric sources/sinks.

So one is left with the following simpler equation:

$$\dot{S} = \pm\dot{W} \tag{2.2}$$

In Figure 2.3, according to Paschedag (2004), one can see some of the interactions of drops of

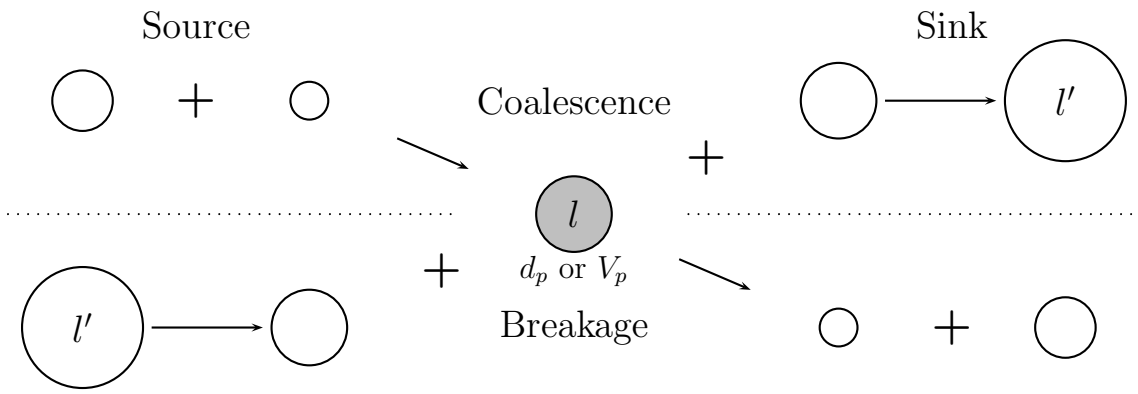

Figure 2.3: Involvement of a certain particle size l in breakage and coalescence and its interpretation in the PBE according to Paschedag (2004)

a certain size and their interpretation as source or sink terms.

The left side of Figure 2.3 displays how a particle of a certain size (inner coordinate l: diameter d_p or volume V_p) can be generated either by the coalescence of two (or more) smaller drops or by the breakage of a bigger one.

Particles of that specific diameter or volume can also be destroyed either by coalescing with another particle, forming a bigger one, or by breaking into small ones and by doing that contributing to the sink side of its size class (right side of Figure 2.3).

One has to take into account that every event (breakage or coalescence) influences more than one particle size class in the PBE. To specify this equation further one has find formulations for each term used. The storage term $\dot{S}$ is the rate of change of the number density function for a particular size class $\partial n(l)/\partial t$ and the source/sink term $\dot{W}$ can be fragmented into the respective source and sink terms, $G_{break}(l,t) + G_{coal}(l,t)$ and $D_{break}(l,t) + D_{coal}(l,t)$. This yields the following equation:

$$\frac{\partial n(l,t)}{\partial t} = \underbrace{G_{break}(l,t) + G_{coal}(l,t)}_{source} - \underbrace{D_{break}(l,t) + D_{coal}(l,t)}_{sink} \tag{2.3}$$

As in this work only drop breakage is investigated, terms for coalescence will not be taken along further. The two breakage terms for the sink and source can be replaced by a formulation as follows. D_{break} as the sink term by breakage can be said to be composed of a breakage rate (breakage kernel) $g(l)$ and the size distribution $n(l,t)$ itself. One can also say that the source by breakage is composed of a breakage rate (breakage kernel), this time of the larger drops $g(l')$, a daughter size distribution $\beta(l,l',t)$ and the number of initial drops generated $v(l',t)$, considered to be two when assuming binary breakage and the size distribution $n(l',t)$.

This leads to equation (2.4):

$$\frac{\partial n(l,t)}{\partial t} = G_{break}(l,t) - D_{break}(l,t) \tag{2.4}$$

with:

$$G_{break}(l,t) = \int_{l}^{\infty} g(l')\,\beta(l,l',t)\,v(l',t)\,n(l',t)\,\mathrm{d}l'$$

$$D_{break}(l,t) = g(l)\,n(l,t)$$

In order to solve the number density transport equation, functions for the breakage rates, daughter size distribution and the number of initial drops have to be determined, either by a phenomenolgical or a stochastical approach. It is necessary to analyse and understand the phenomena leading to drop breakage because there is no satisfactory description so far (Maaß et al., 2010).

2.3 Modelling of drop breakage

In this work only some terms of the breakage term in the PBE can be investigated further. The focus will lay on formulations for the breakage rate $g(l)$ or $g(l')$, and a short look will be taken on the number of daughter drops generated by the first breakage event $v(l',t)$.

The breakage rate as well as the number of initial daughter drops is a function of many parameters, for example of the system properties like viscosity, interfacial tension and density, drop size, local energy dissipation, geometrical factors, ionic strength, and so on. Some of the models for breakage rate or number of initial daughter drops include the dependency on some of those parameters and different models sometimes include different parameters. Various researchers have investigated the influence of the energy dissipation (Maaß et al., 2010), the drop size (Zillmer, 2010; Maaß et al., 2010), the ionic strength (Zillmer, 2010) and viscosity (Calabrese et al., 1986) as well as interfacial tension.

2.3.1 Breakage rate

Numerous authors have been working on the determination of a theoretical model for drop breakage and their results partly predict contradictory behaviour. As an example three of the more prominent models have been chosen to be briefly summarised here. Here only the breakage rate will be considered.

Coulaloglou and Tavlarides (1977): They consider the breakage mechanism of drop-eddy collisions to be the dominating one. Some of its characteristics could already be seen in Section 2.1 and will be described more exactly now.

It is said that an oscillating deformed drop will break if its kinetic energy E_d, transmitted to it by drop-eddy collissions, is greater than its surface energy E_c.

The authors work under the assumption that drops are moving in a locally isotropic, turbulent velocity field.

They define the breakage rate as follows:

$$g(l) = \left(\frac{1}{\text{breakage time}}\right) \times \begin{pmatrix}\text{fraction of}\\ \text{drops breaking}\end{pmatrix} = \frac{1}{t_B} \times \frac{\Delta_B N(l)}{N(l)} \tag{2.5}$$

In equation (2.5), the fraction of drops breaking (breakage probability) is assumed proportional to the fraction of turbulent eddies with a kinetic energy higher than the drops' surface energy colliding with the drop. The breakage time is estimated by applying theories of particle separation in turbulent flows.

When replacing the inner coordinate l with the volume of the particle V_p, an equation for the breakage rate can be written with C_1 and C_2 as dimensionless constants:

$$g(v) = C_1 v^{-2/9}\, \varepsilon^{1/3} \exp\left[-\frac{C_2\, \gamma}{\rho_d\, \varepsilon^{2/3}\, V_p^{5/9}}\right] \tag{2.6}$$

The authors later adjusted this equation by adding a damping factor α, thereby accounting for the effect of drops on the local turbulent flow at high holdup fractions.

Alopaeus et al. (2002): By refining an already developed model with the probability theory by Narsimhan and Gupta (1979), Alopaeus et al. (2002) developed the following equation with C_3, C_4 and C_5 as parameters:

$$g(d_p) = C_3\, \varepsilon^{1/3}\, \mathrm{erfc}\left(\sqrt{C_4 \frac{\gamma}{\rho_c\, \varepsilon^{2/3}\, {d_p}^{5/3}} + C_5 \frac{\eta_d}{\sqrt{\rho_c\, \rho_d}\, \varepsilon^{1/3}\, {d_p}^{4/3}}}\right) \tag{2.7}$$

The basic assumption for the model and the one it is based on is, that drop-eddy collisions behave like a Poisson process. Alopaeus et al. (2002) modified the model by taking the viscous force of fluid inside the drop into account. Unlike the model of Coulaloglou and Tavlarides (1977), which has two parameters, the model of Alopaeus et al. (2002) has three.

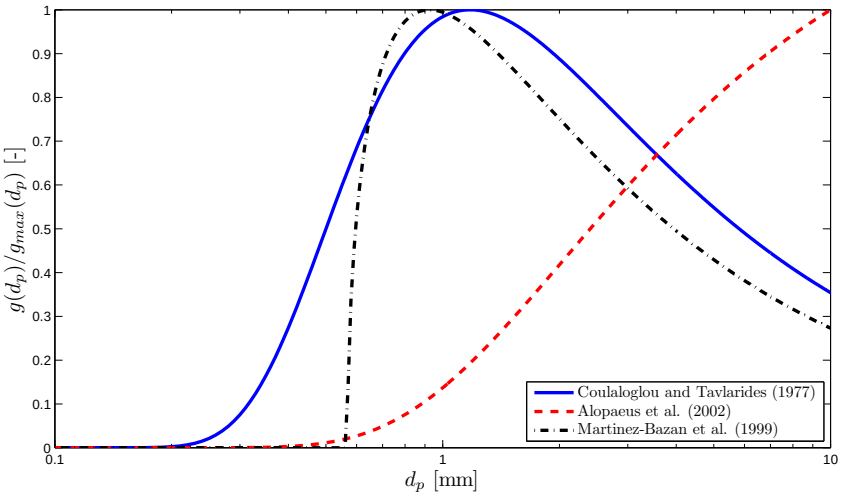

Figure 2.4: Visualization of three breakage kernels

Martínez-Bazán et al. (1999): They state, that drop breakage occurs when the surface of the drop is deformed significantly enough by the continuous phase. The drop breaks if its surface energy is exceeded. It becomes evident that there is a critical drop diameter below which no breakage occurs. This critical diameter increases with increasing energy dissipation rate or decreasing interfacial tension.

They end up with the following equation (2.8) with C_6 and C_7 as parameters:

$$g(d_p) = \frac{1}{t_B} = C_6 \frac{\sqrt{C_7 \, (\varepsilon \, d_p)^{2/3} - \dfrac{12\,\gamma}{\rho_c \, d_p}}}{d_p}. \tag{2.8}$$

Summary: A visualization of all the models can be seen in Figure 2.4, where the normalised breakage rate is displayed over the drop diameter. Two of the models (Coulaloglou and Tavlarides, 1977; Martínez-Bazán et al., 1999) have distinct maxima and one does not (Alopaeus et al., 2002). Also it can be seen that the model of Martínez-Bazán et al. (1999) has a breakage rate ($g(d_p)$) equal to zero until a critical drop diameter ($d_{p\,crit}$) is reached and that is then increasing rapidly.

The definition of the breakage rate by Coulaloglou and Tavlarides (1977) with breakage time and breakage probability allows an experimental approach towards testing the models and their behaviour. All the models have empirical constants and they only include some of the system properties mentioned above. Coulaloglou and Tavlarides (1977) did not include, either the viscosity of the dispersed or continuous phase, or the density of the continuous phase. Viscosity of the dispersed phase is included in the model of Alopaeus et al. (2002) while the density of

the continuous phase is included in the model of Martínez-Bazán et al. (1999). Though not directly including some of the influencing factors, the models can be fitted (through adjustable constants C_i) to more or less match experimental results.

2.3.2 Number of initial daughter drops

Many authors consider the number of initial drops to be two, calling it binary breakage. This is partly contradictory to experimental results showing a number of daughter drops higher than two. Authors like Bahmanyar and Slater (1991) consider the number to be dependant on the drop diameter and a critical drop diameter (see equation 2.9), while Kuriyama et al. (1995) states it to be proportional to the drop diameter and the viscosity fraction (see equation 2.10).

$$v = 2 + 0.9 \left[\frac{d_p}{d_{p\,crit}} \right] \tag{2.9}$$

$$v \propto \sqrt{\frac{\eta_d}{\eta_c}}\, {d_p}^{0.455} \tag{2.10}$$

2.4 Experimental investigations on drop breakage

Drop breakage and coalescence always occur together, and there are experimental setups in a stirred vessel where the interaction can be examined. There are experimenters who investigate drop breakage in stirred vessels with hindered coalescence (dilute system or surfactants) and there are others who investigate the interaction directly. Others investigate breakage events by single drop experiments.

Konno et al. (1983) for example directly observed drop breakage events in a stirred vessel, using high-speed photography with up to 4000 fps. They recorded the breakage time, the drop path and the number of drops per breakage event. The dispersed phase fraction thereby lay lower than 0.2%. Bahmanyar and Slater (1991) observed breakage of single drops using a rotating disc contactor. They investigated the number and distribution of daughter drops as well as the breakage probability. Single drop breakage events in a stirred vessel (drops introduced by loop flow) were investigated by Kuriyama et al. (1995). They analysed the influence of viscosity on the number of daughter drops. Another digital high-speed imaging technique was used by Andersson and Andersson (2006) when they investigated the dynamics of bubble and drop breakage. The breakage time, the daughter size distribution as well as the breakage probability were determined. Galinat et al. (2005) investigated swarms of drops as well as single drops in a pipe flow. The breakage probability, the number of daughter drops as well as the daughter

drop distribution was ascertained.

A more extensive summary of experimental procedures was given by Maaß et al. (2010). In Table 2.1 some of the different methods are laid out, (SW) meaning swarm investigation and (SD) single drop.

Table 2.1: Summary of experimental procedures

Reference	Set-up	Investigated properties
Konno et al. (1983)	Stirred vessel	(SW) Breakage time, drop path, number of drops per event
Bahmanyar and Slater (1991)	Rotating disc contactor	(SD) Number and distribution of daughter drops, breakage probability
Kuriyama et al. (1995)	Stirred vessel	(SD) Number of daughter drops
Andersson and Andersson (2006)	Static mixed reactor	(SW) Breakage time, daughter size distribution, breakage probability
Galinat et al. (2005)	Pipe flow	(SD)(SW) Breakage probability, number and distribution of daughter drops

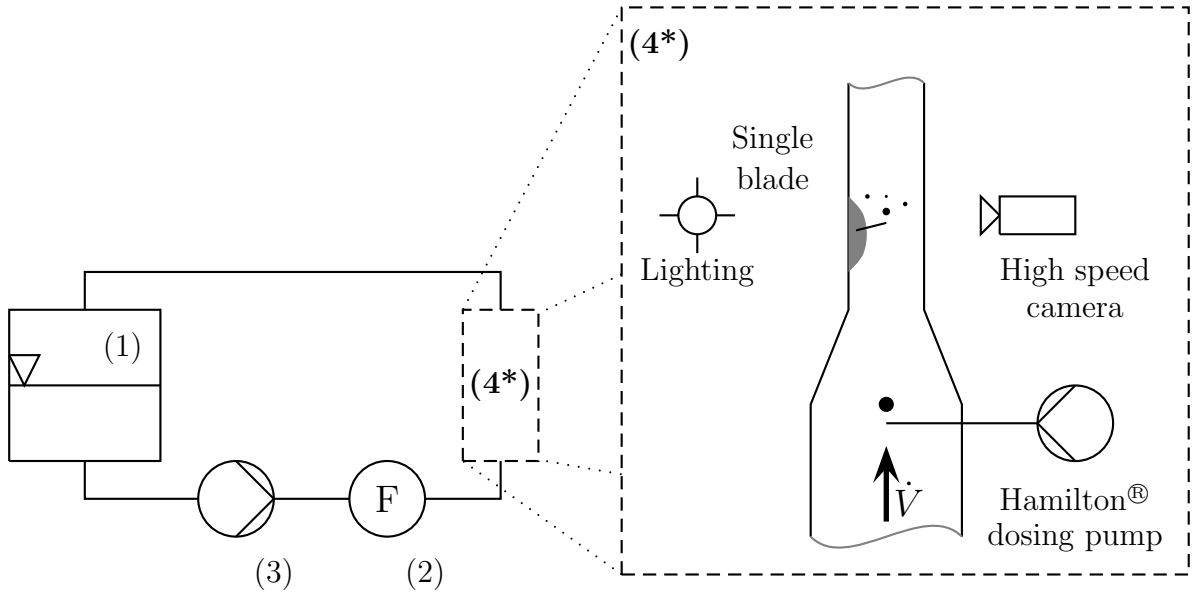

(a) Flow sheet

(b) Breakage channel detailed

Figure 3.1: Simplified set-up with flowsheet (a) and a detailed view of the channel (b)
(1) Storage tank, (2) Flowmeter, (3) Rotary pump, (4*) Breakage channel

3 Materials and methods

3.1 Experimental set-up

The foundation of all the experimental work done here is the single drop breakage cell, first thought up by Maaß (2005) and later refined by Zillmer (2010). Only a short overview of the current setup can be given here, a more detailed description, also of the refinements, can be found in Zillmer (2010).

The approach taken here is the examination of a single drop breakage event where coalescence can be practically neglected.

Figure 3.1 shows a simplified flow diagram. Deionised water (500 l) is stored in a tank (1) that has a volume of 1 m^3. The water is then pumped through flexible pipes to a flow meter (2), where the flow rate is displayed, by a rotary pump (3). The flow rate measurement works by magnetic inductive flowmeter. An amount of 80 g NaCl (sodium chloride) has to be added to 500 l deionised water to increase the conductivity to a value of 80 mS/cm. The flowrate of the rotary pump (3) is controlled by a frequency generator (not shown in the figure).

The rectangular breakage channel (4*) consists of two parts, one made of acrylic glass and multiple inner areas where the drops are generated (as explained below), and a part (30 mm x 30 mm) made of glass where one single blade of a Rushton turbine ($d = 0.08$ m) is mounted. The drops

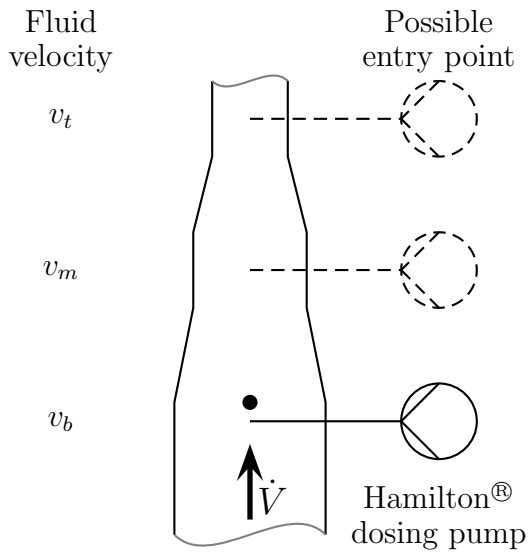

Figure 3.2: Detailed view of the entry section of the channel

are being generated with glass canula or steel needles mounted in the channel wall via an opening. A Hamilton® dosing pump PSD/3 controlled by computer programm is responsible for the introduction of the drops into the continuous phase out of a reservoir.

Figure 3.2 shows a more detailed view of the entry section into the channel. The needles/cannula can be positioned at three different levels of the channel wall, each corresponding to another fluid velocity inside the channel ($v_b = 0.09\,v_0$, $v_m = 0.17\,v_0$ and $v_t = 0.46\,v_0$). These velocities are determined by the flowrate of the continuous phase ($\dot{V}$) and the cross-sectional area of the channel at that entry point (for further information see Zillmer, 2010).

At the top part of the channel high speed cameras and lighting equipment can be mounted in order to observe the breakage events. That equipment can also be mounted at the bottom part of the channel to observe the introduction of drops into the flow for the motherdrop analysis. Table 3.1 displays some technical specifications of the equipment used.

In the single drop breakage cell the flow velocity field has to be equal to the velocity field in a stirred vessel for the results to be comparable. The velocity difference between the stirrer blades and the surrounding fluid at a given rotation speed (400, 550, 700 1/min) has to be taken into account. The product of the velocity difference and the free-stream-area is the flow rate and the free-stream-area is the inner area of the channel minus the area of the blade. The detailed calculations leading to Table 3.2 can be found in Maaß (2005).

Table 3.1: Technical specifications

Description	Product number	Producer
High speed CMOS camera	MV-D752-160	Photon Focus®
Telecentric lens	Sill Correctal T 3.0	Sill
Normal objective lens	Pentax TV-lens H1212B	Pentax
Hamilton® dosing pump	PSD/3 Syringe Pump	Hamilton® Company
Rotary pump	HYGIA 1/30 A	Hilge Bodenheim
Frequency generator	-	Danfoss
Flow meter (electromagnetic)	Aquaflux 410 K	Krohne
Dosing needles	(22s/51/pst3/tapN) (22s/51/pst5/tapN) (22/51/pst3/tapN) (33/51/pst3/tapN)	Hamilton® Company
Custom-built glass cannulas	-	-

Table 3.2: Summary of flow velocities and flow rates, comparison vessel/channel (Maaß, 2005)

Symbol	Property name	Value			Unit
n	Stirrer speed equivalent	400	550	750	[1/min]
Vessel					
ε	Energy dissipation rate	0.14	0.36	0.73	[kW/m^3]
ε_{max}	Maximum local energy dissipation rate	6.22	16.18	33.35	[kW/m^3]
v_{tip}	Stirrer tip velocity	1.05	1.44	1.83	[m/s]
v'_{max}	Maximum fluctuation velocity	0.32	0.44	0.55	[m/s]
Channel					
ε	Energy dissipation rate	0.16	0.41	0.85	[kW/m^3]
ε_{max}	Maximum local energy dissipation rate	5.84	15.30	31.43	[kW/m^3]
v_{tip}	Stirrer blade tip velocity	1.59	2.19	2.79	[m/s]
v'_{max}	Maximum fluctuation velocity	0.48	0.66	0.84	[m/s]
v_0	Flow velocity at stirrer blade	1.11	1.53	1.94	[m/s]
$\dot{V}$	Overall flow rate	2316	3185	4054	[l/h]

Table 3.3: System properties of the dispersed phases

Symbol	Property name	Value	Unit
Toluene			
ρ_d	Density at 20 °C	870	kg/m^3
c_{dye}	Dye concentration	0.075	g/l
γ_d	Interfacial tension at 25 °C	36	mN/m
$\gamma_{d\ dye}$	Interfacial tension (with dye) at 25 °C	32	mN/m
η_d	Viscosity	0.55	mPa s
Paraffin oil (10)			
ρ_d	Density at 25 °C	806	kg/m^3
c_{dye}	Dye concentration	0.075	g/l
γ_d	Interfacial tension	42	mN/m
$\gamma_{d\ dye}$	Interfacial tension (with dye)	44	mN/m
η_d	Viscosity	8	mPa s
Paraffin oil (100)			
ρ_d	Density at 25 °C	850	kg/m^3
c_{dye}	Dye concentration	0.075	g/l
γ_d	Interfacial tension at 25 °C	48	mN/m
$\gamma_{d\ dye}$	Interfacial tension (with dye) at 25 °C	55	mN/m
η_d	Viscosity	125	mPa s
Petroleum			
ρ_d	Density at 20 °C	790	kg/m^3
c_{dye}	Dye concentration	0.075	g/l
γ_d	Interfacial tension at 25 °C	42	mN/m
$\gamma_{d\ dye}$	Interfacial tension (with dye) at 25 °C	38.5	mN/m
η_d	Viscosity	0.65	mPa s

It was researched and ensured that the hydrodynamic conditions, for example the energy dissipation and the fluid velocity, are similar in the single drop breakage cell and in a stirred vessel (Maaß, 2005). This set-up allows the determination of the behaviour of systems during drop breakage and the experimental results found can be integrated into the models mentioned in Subsection 2.3.1. The system properties of the dispersed phases used are displayed in Table 3.3.

Table 3.4: Summary of experiments

Dispersed phase	Velocity v_0	Mother drop diameter d_p	Description
Toluene	1.5 m/s	1011 µm	motherdrop analysis, breakage analysis at 822 fps, full image size, evaluation of smaller pictures
		1011 µm	motherdrop analysis, breakage analysis at 1450 fps, half the image size, evaluation of half of the pictures
Paraffin oil (10)	1.5 m/s	1023 µm	motherdrop analysis, breakage analysis at 822 fps, full image size
Paraffin oil (100)	1.5 m/s	1000 µm	motherdrop analysis, breakage analysis at 822 fps, full image size
	1.5 m/s	$\leq$ 750 µm	multiple motherdrop analyses with toluene, paraffin oil (10) and (100) and petroleum

3.2 Experimental procedure

A short summary of the research is given in Table 3.4. The influence of the system properties on drop breakage was investigated by using three substances as dispersed phase (see Table 3.3) at 822 fps and doing drop breakage experiments. The influence of the framerate on the number of initial daughter drops was investigated by increasing the experiments' framerate to 1450 fps and by bisecting the viewed area. By conducting multiple motherdrop analyses, the influence of the type of the needle and the entry point into the channel on the drop diameter at creation was determined.

3.2.1 Motherdrop analysis

Prior to all single drop breakage experiments, a motherdrop analysis was carried out in order to ensure the steady injection of equally sized drops into the flow. Therefor high speed images (822 fps) of the injection point were taken with a telecentric and a normal object lens and processed. Experience showed that 200 injection events are sufficiant to ensure the quality of the drops.

The images aquired through this method were then analysed. As a result the motherdrop distribution is calculated and determines if the breakage analysis can be conducted.

The image processing is fully automated with help of the commercial program MATLAB®. A

detailed description can be found in Zillmer (2010) and will not be described in great detail further. Only a short summary should be given.

All the images taken are loaded into a MATLAB® tool, where a region of interest and a reference length have to be defined.

Then an image-subtraction takes place to get the changes between a background image and an image showing a drop. Subsequently, the remaining picture undergoes a scaling procedure where all the grey values are expanded into a 255 value range again. Then this scaled picture is binarised, it is converted into a black and white picture at a threshold grey value. All images showing a drop are then evaluated for drop size (in pixel and mm) and eccentricity. Those values are displayed in an Excel chart after image processing.

3.2.2 Single drop breakage analysis

After the quality of the drop generation is ensured the actual breakage analysis can be conducted. Maaß (2005) showed that approximately 1000 events, using this setup and parameter set, should be recorded for the result to be statistically meaningful (can be accepted when the measured value, here for example breakage probability, approaches its mean value by cumulative calculation). Here it is important to catch each and every event (breakage or no breakage) to not alter the results.

Subsequent to recording all the drops, the images are given to a MATLAB® tool for further examination. The breakage analysis procedure is devided into two parts: a cutting and sorting part, and the actual image processing part.

Due to a peculiarity of the image capturing, the images saved on the harddisk are not always correctly ordered. Additionally, many images do not contain any drops at all. The task of the cut and sort procedure is to cut the images down to the region of interest, sort them into the correct order and dismiss all the images not containing any drops.

The remaining pictures then undergo the actual quantitative analysis where the area of the objects, their location and their number are recorded. This means that the image substraction, the rescaling to 255 grey values, as well as the transformation to black and white has to occur. Additionally, when a drop breaks from one frame to another, the breakage time and the breakage location is calculated. When calculating the breakage time Zillmer (2010) defines t_B to be the interval between the time when the drop passes the stirrer blade and the time when more than one drop is visible on the picture. It is determined by dividing the frame number by the framerate. The breakage location is calculated by averaging the x- and y-location of the centers of gravity of all the daughter drops after first breakage. To ensure that only valid drops

(correct diameter) are analysed, the routine checks a mass balance, based on a mean diameter one has to give it as input before starting the calculation. This mean diameter comes from the motherdrop analysis. It is transformed into an equivalent drop volume and then compared with an equivalent drop volume, calculated from the areas on the images. The accepted range is $V_p \pm 25\%$.

Again the resulting values are displayed in an overall Excel chart and every sequence has additional information stored in a detailed chart.

4 Theoretical and experimental preexaminations

The task was to prepare the set-up for the required accuracy for dealing with small ($200 - 500$ µm) drops. This included an examination of drop generation and drop breakage events.

4.1 Drop generation

The construction of the needle system can be reviewed further in Maaß (2005). When considering drop diameters smaller than 500 µm the needles tips have to be very small (in order of magnitute of the drops themselves).

Needles: All the thin glass needles used by Maaß (2005) and Zillmer (2010) were manufactured by elongation thinning using a Bunsen burner. That lead to glass needles with quite a small inner and outer diameter of about $d_{inner} \approx 200$ µm and $d_{outer} \approx 350 - 400$ µm. Every hand-made needle therefore was unique in its measurements and was able to steadily produce drops of a certain diameter. This effect is not desirable because manufacturing has to be reproducable, i.e. in case the tip breaks during assembly.

The accuracy in industrial manufacturing of steel and glass needles in series is considered to be much higher than the accuracy of hand-made manufacturing. In order for the results of the experimental research to be reproducable, also by other research groups, every piece of equipment should be standardised. This also includes the dosing needles.

Heat shrink tube: Heat shrink tube was used as a connection between the needle and the tubing leaving the dosing pump. After disassembling some of the needles it could be seen that the chemicals used (especially toluene) influenced the heat shrink tube and that the connection was not fast enough. That manifested itself in a considerable error in the motherdrop analysis of the smallest drops. One could notice a retreat of the fluid level in the glass needle due to small variations of the position of the tubing (see Figure 4.1 for clarification).

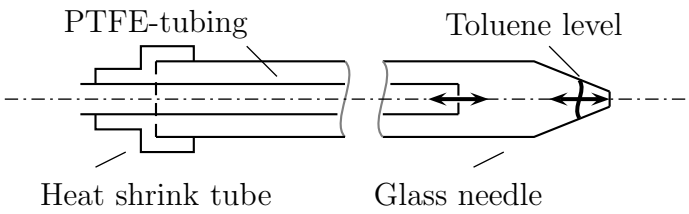

Figure 4.1: Variation of fluid level in the needle tip

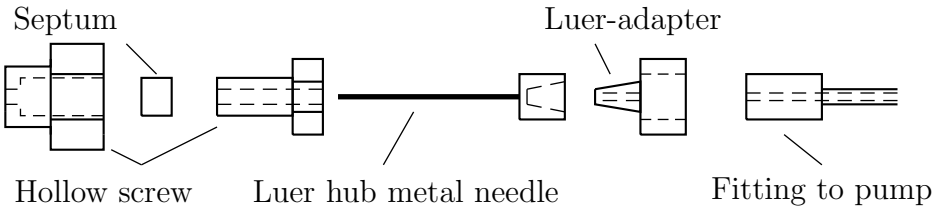

Figure 4.2: Schematics of standardised needle set-up

It was therefore decided to use fittings and adapters by Hamilton® Company in order to get rid of that fluid level variation and for standard industrial steel needles to be applied to the task. The needle was then stuck through a septum (mounted in a hollow screw) into the channel. Details can be viewed in Figure 4.2.

Two phase drop generation or mechanical rocking motion mechanism: Another possibility to create small drops would be to use a two phase drop generation procedure as used by other experimenters in the laboratory. Two Hamilton® pumps would generate small droplets of toluene in bigger droplets of water and those would be injected into the continuous water flow. This was dismissed because of experiences in drop generation, difficulties in creating the drops in drops and the fact they would be too big to begin with because the T-connection has an inner diameter that is too wide. Another idea to generate small drops is to use a mechanical lateral rocking motion generator to throw the drops off the needle into the water.

4.2 Analysis of the breakage event

Preexaminations concerning the camera and objective lens set-up as well as the automated image processing were also conducted. First of all the photography process is still very subjective. The experimenter gets to decide which drops are being used for processing and, be it willingly or not, alter the results. In spite of the dye the drops are still hard to see because of their high velocity. The aim must be to have an image resolution as high as possible and to reduce image defects and thus achieve a high accuracy in data processing.

4.2.1 Image resolution

When trying to take pictures of smaller drops with satisfactory accuracy one has to increase the image resolution. Image resolution is directly linked to the objective lens and its parameters as well as its mounting and distance to the object. At this time, the main problem is the limited maximum data rate of the transfer from camera to the computer.

Table 4.1: Maximum theoretical data rates according to Stemmer® Imaging

Hardware part	Value	Unit
Photon Focus® camera MV-D752-160	150	MB/s
Frame grabber MicroEnable III	264	MB/s
Applet Dual area gray	170	MB/s
Applet Single area gray	220	MB/s

Because the overall object size (in mm) was fixed by earlier experiments, the camera could only be positioned so that this image size is projected onto the dimensions of the CCD-chip in the camera (752 x 582 Pixel^2). Also the framerate to be used was fixed by earlier experiments at 822 frames per second. One can calculate the data rate at which the camera would have to transfer the data to the computer in order to achieve such a resolution. Considering the hardware constraints shown in Table 4.1 one can see that such an increasing was not possible with distance rings and the lens used. The camera Photon Focus® MV-D750-160 is not capable of transfering faster than 150 MB/s. In previous experiments the data rate was tuned up to 141 MB/s at a picture size of 608 x 286 Pixel^2 at 822 fps.

The resolution is limited by the area viewed and the framerate, both creating the data rate. So in order to increase the resolution one has two possibilities which will be considered in detail below:

(i) decreasing the viewed area or framerate by means of image reduction or reduction of the distance

(ii) increasing the data rate by means of aquiring new hardware.

(i) Viewed area, distance, framerate: One way to increase the image resolution is to mount a distance ring between camera and objective lens, thereby allowing a smaller distance between camera and object, leading to a higher image resolution, leading to a decreased viewable area like mentioned above.

Experiments, finding the theoretical maximum resolution with a given distance ring and the object lens used ($\approx$ 10 px/mm in previous experiments) were conducted.

- no ring corresponds to 8.8 Pixel/mm
- 1.4 mm ring corresponds to 17.7 Pixel/mm (already in use)
- 1.9 mm ring corresponds to 21.2 Pixel/mm

A second possibility is the reduction of the object dimensions or the framerate. When presuming the drop entry to be symmetrical, mirrored at the stirrer disc plane, one could only observe one half of the prior area, but with increased resolution. The limit of what one could achieve is coupled with the biggest dimension of the area viewed. This

dimension would have to be projected to the biggest dimension (752 Pixel) of the CCD-Chip. When not reducing the biggest dimension of the area viewed a resolution of 12.5 Pixel/mm could be achieved. When the limitation of the camera-computer-link can be exceeded, one could reach the maximum resolution of the distance ring used.

The reduction of the frame rate directly influences the data rate but would significantly alter the results of the experiments because of influencing the time-resolution of the breakage events.

(ii) Hardware related: Another possibility was to use two of those Photon Focus® cameras in parallel at one frame grabber card, but the hardware constraint coming in here is the Dual area gray hardware applet with its maximum at 170 MB/s. It is not possible to generate an increase in resolution using that applet. An improved frame grabber (MicroEnable IV) would be capable of using another dual area gray applet with a higher data rate.

Using a triggering mechanism it would be theoretically possible to utilize two computers, each with a frame grabber card and a camera attached to it, running the Hardware applet Singe area gray with 220 MB/s. In this case the resolution could be increased to the maximum value corresponding to the distance ring used.

By doing that, one would introduce either error or further calculation complications having to do with perspective (see Section 4.2.2).

The first of the two always includes a change of predefined parameters (framerate or area viewed) for one cannot exceed the hardware limitations of the camera-computer-link. Only the second possibility contains in itself an increased resolution at constant predefined parameters.

4.2.2 Image defects

The usual lenses used are entocentric lenses that utilize the natural perspective, leading to pictures like the human eye is used to. Objects that have the same dimension, but are at different distances to the lens/eye are displayed as if they had different dimensions, the object further away is displayed as if it was smaller, so making it possible for the brain to judge distances. That is because the optical path of the entering main rays is not parallel. For further information about object lens perspective see Thöniß (2006).

In this case that means that one cannot observe the complete interior of the channel. In one alignment extreme (see Figure 4.3) the top parts are missing and in the other alignment the glued side walls are visible in the picture disturbing the image processing and giving completely impossible results (i.e. the drops break outside the channel). The alignments are generated by

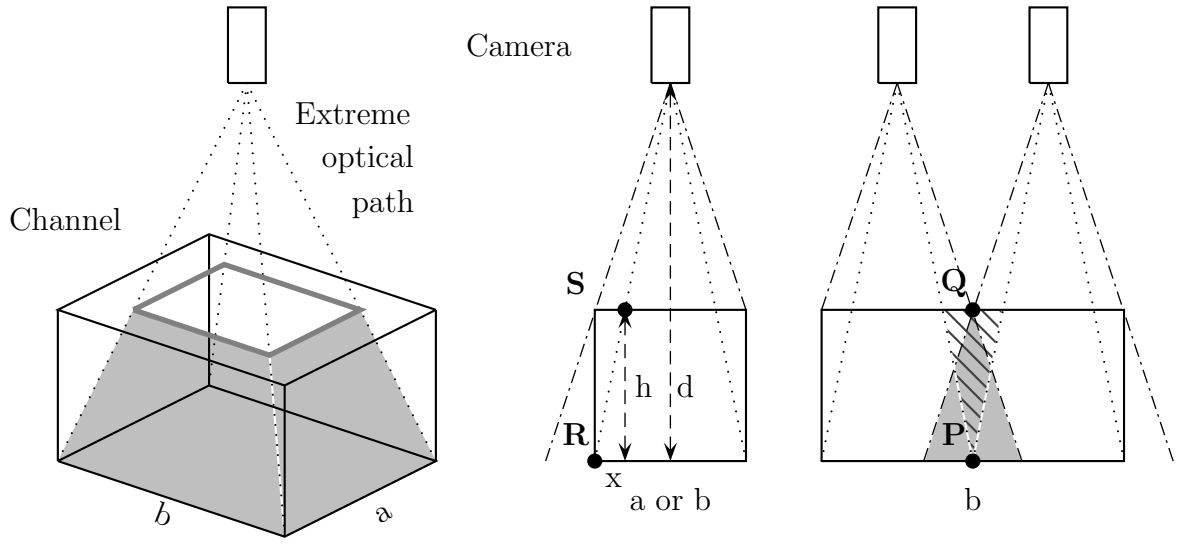

(a) 3D schematics of channel, one camera

(b) Projection and visibility

Figure 4.3: Visualisation of breakage location projection

adjusting the region of interest to either the channel dimensions visible on the back side or the front side.

So the breakage location is always a projection of the real breakage location onto the channel back wall, generating a two-dimensional graph. This means that drops at different locations may generate the same projection when they are aligned on one particular optical path line, as can be seen in Figure 4.3. Point R and S, and every point on a straight line between them, are projected to the same location at the back wall.

One can calculate a value of the maximum error (vertical length between the real positions of points R and S when considering b as basis coordinate) using the theory of similar triangles (result to be seen in equation 4.1).

$$x = \frac{b/2 \times h}{d} \approx 7.5\text{mm} \tag{4.1}$$

As mentioned before in Section 4.2.1, the use of two cameras complicates this fact even further. The two optical paths leading through point P visualize the setting of no overlay. Every event above that point P (in the dashed region) is invisible to either one of the cameras.

When considering the overlay setting visualized by point Q one can easily see that all events below that point (filled region) are projected to different locations, according to which camera is used. This effect is at its maximum at point Q itself.

At last one has to take into consideration the distortion at the edges of the images. All the pictures show a barrel distortion, so that parallel lines of the object (i.e. channel walls) are no

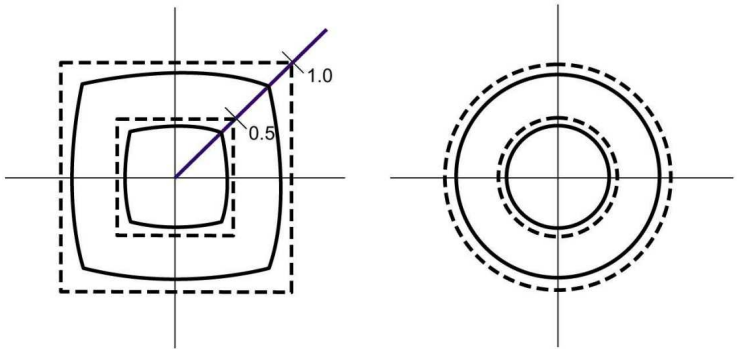

Figure 4.4: Clarification of distortion according to Thöniß (2006)

longer parallel in the picture. Figure 4.4 according to Thöniß (2006) shows this situation. The dashed lines would be the projection in the ideal case and the solid lines show the distortion. For further extensive information on image defects see Thöniß (2004, 2006).

4.3 Conclusion

The purchase of the more expensive components like new personal computer, the improved frame grabber card, another better camera, a triggering mechanism or a telecentric lens is postponed until proven that the drop generation leads to adequate drops.

The standardisation of the drop inlet into the channel was done and industrially produced metal needles are in use. Distance rings were in use already when the project was started, though not the widest ones.

5 Experimental results and discussion

The influence of the system properties was investigated by using 1 mm drops of the three different substances toluene, paraffin oil (10) and paraffin oil (100) (see Table 3.3). Additionally the data was compared to petroleum. The experiment with petroleum was conducted by another experimenter in the laboratory.

In the experimental investigation more than two daughter drops are often seen after the first breakage event. The theory of binary breakage was tested with toluene by increasing the framerate and thereby the time resolution of the image taking process. Only one half of the area was analysed due to a limitation in the maximum data rate and simulations with CFD showed an almost equal distribution of the energy dissipation rate (Maaß et al., 2009). The number of initial daughter drops was then compared to the values of the experiment with 822 fps.

In order to investigate small drop diameters, the possibilities of drop generation using this set-up and those dispersed phases were identified. This was done by adjusting the settings of the Hamilton® dosing pump, changing the entry point and using different needles.

5.1 System properties

Prior to each breakage experiment a motherdrop analysis was conducted to ensure a steady supply of drops with a given diameter. Then the breakage events were recorded and evaluated.

5.1.1 Motherdrop analysis

In the process included was the examination of 200 drops shortly after leaving the cannula/needle with the high-speed camera at 822 fps, using two different object lenses, one regular and a telecentric lens with a much higher magnification. Both lenses were used in the experiment with toluene, the other motherdrop analyses were conducted using only the telecentric lens. The following paragraphs show the result of those motherdrop analyses.

Toluene, 1 mm: The toluene drops were generated using the glass cannula. Figure 5.1 shows a graph for each analysed drop. This plot of the relative number of drops against the deviation from the mean diameter shows one distinct maximum, as desired.

Almost all drops (99.5%) are in the interval of ±5% around the mean diameter. Those drops could be used for carrying out the breakage experiment. When comparing the accuracy and

sensivity against errors of the telecentric and normal entocentric lens, one sees that the telecentric lens shows less sensitivity against errors of the manual input and is also more accurate (see subsection 5.4). The use of the telecentric object lens could achieve a resolution of about 100 pixel/mm whereas the use of the normal lens yielded a resolution of about 10.91 pixel/mm. Being at 1011 µm, the mean drop diameter is very close to the desired value of 1 mm.

Paraffin oil (10), 1 mm: A metal needle was used to generate the drops. This lead to drops with 92.7% in an interval of ±5% around the mean diameter. Though not being as narrow as for the 1 mm toluene drops, the drop size distribution (see Figure 5.1) was still narrow enough.

The images were taken with the telecentric lens because of its accuracy and resolution and the exact mean diameter achieved was 1023 µm, still being close enough to 1 mm.

Paraffin oil (100), 1 mm: This drop size was also generated using a glass cannula. The mean drop diameter is 1001 µm and 92.6% of the drops are in an interval of ±5% around the mean diameter.

(a)

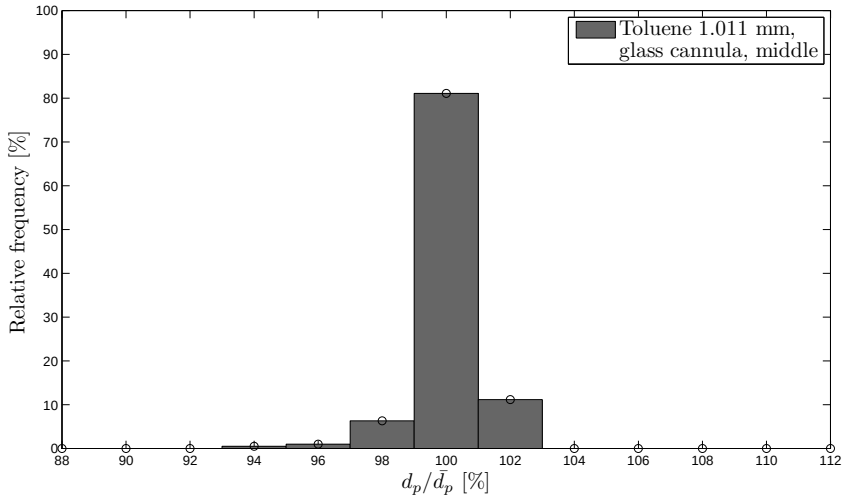

(b)

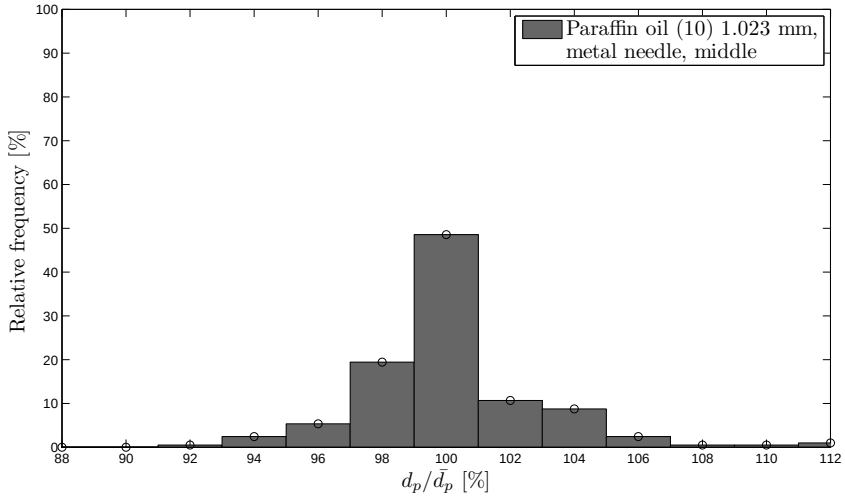

(c)

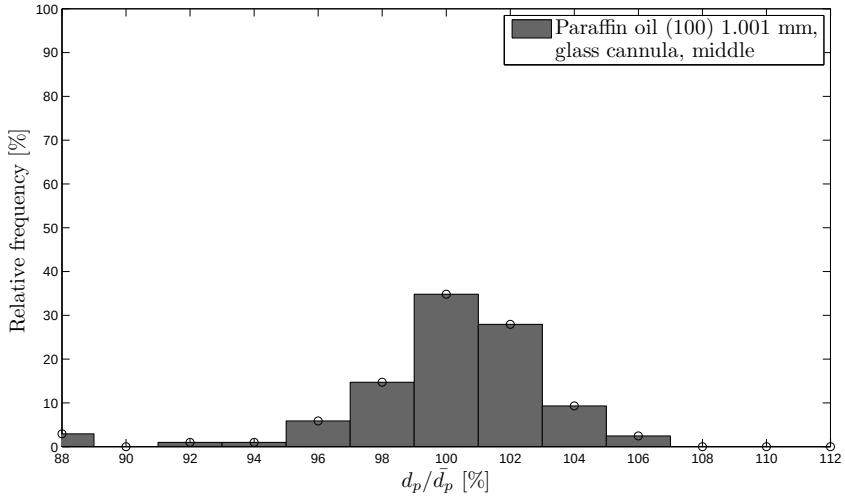

Figure 5.1: Histograms for the 1 mm droplets of (a) toluene, (b) paraffin oil (10) and (c) paraffin oil (100)

(a)

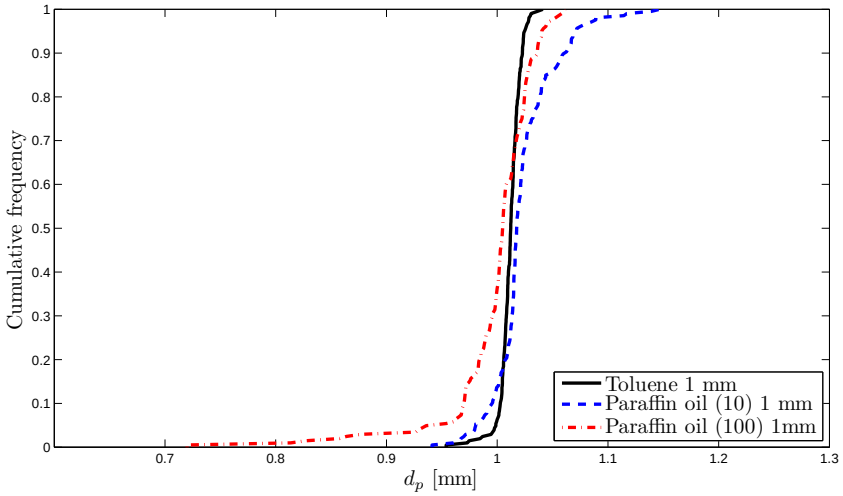

(b)

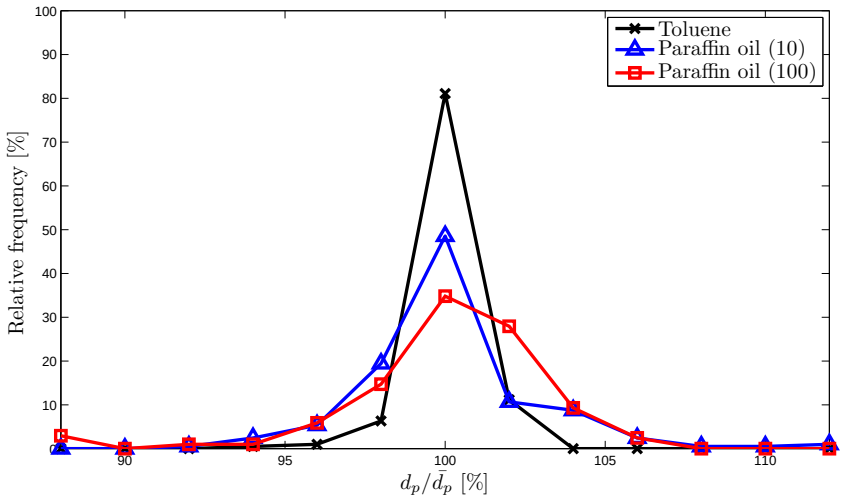

Figure 5.2: Comparison of the three substances at 1 mm by means of cumulative distribution (a) and transformed histogram (b)

Comparison: As a comparison between toluene and the two paraffin oils, Figure 5.2(a) shows all three cumulative distributions in one diagram. It is evident, that the dispatch of toluene drops from the glass cannula was better than that of the paraffin oil (10) drops from the metal needle. All three histograms were transformed into a line plot with markers and can be seen in Figure 5.2(b). Every one of those three settings could be used for a breakage investigation. The values of the mean diameter and the standard deviation are displayed in Table 5.1.

Table 5.1: Comparison of the motherdrop analyses

	$\bar{d}_p$ [mm]	σ [mm]	σ [%]	Needle type, entry point
Toluene	1.011	0.010	0.96	glass cannula, m
Paraffin oil (10)	1.023	0.028	2.73	metal needle, m
Paraffin oil (100)	1.001	0.040	3.95	glass cannula, m

5.1.2 Breakage analysis

After making sure that the generated drops are sufficient for a breakage analysis, the following results could be achieved. The focus lay on the breakage probability, the breakage time, the breakage location and the number of initial drops after the first breakage event. To calculate the breakage rate ($g(d_p)$), the breakage probability (P) and the breakage time (t_B) have to be determined as described in section 3.

Breakage probability: In Figure 5.3 the cumulative mean is displayed over the number of sequences. It can be seen that the mean approaches its stationary (final) value.

Toluene has the highest breakage probability of all the tested substances at these settings and paraffin oil (100) has by far the lowest at a value of one half of the others. The breakage probabilities of toluene, petroleum and paraffin oil (10) are in a close range compared with paraffin oil (100) which has the highest viscosity. The change of the viscosity from approximately 0.6 mPa s to 8 mPa s did not seem to have a great influence on the breakage probability. Further increase to approximately 125 mPa s however lead to a noticable decrease of breakage probability. The interfacial tension of paraffin oil is also the highest with 55 mN/m compared to toluene with 32 mN/m. The density does not vary much. Though the interfacial tension has an influence on the stability of the drop and the energy needed to break it, no influence can be observed between toluene and paraffin oil (10) where the difference of interfacial tension is 10 mN/m. But an influence is seen between all substances and paraffin oil (100) where the difference is in the same order of magnitude. One possible explanation could be that a critical value of interfacial tension was exceeded by the paraffin oil (100) and it shows different behaviour because of that. Another explanation could be that a certain critical value of the viscosity was exceeded by paraffin oil (100). It also seems that the breakage mechanism might have changed between paraffin oil (100) and the other substances.

Breakage time: Figure 5.4 shows a histogram of the breakage time with a β-Distribution fitted to it. The arithmetic mean values of the breakage time and the maximum value of the distribution are also shown. It can be seen that the shape of the distribution fits the data quite

well. Not being a good representation of the data, the arithmetic mean is not used as breakage time any longer (for further information see Zillmer, 2010; Maaß et al., 2010).

It can be seen that the breakage times of toluene, petroleum and paraffin oil (10) are very similar (around a value of 6 ms) while the high viscosity paraffin oil (100) has a value almost twice as much. This behaviour can also be seen when comparing the mean values of the breakage time, where paraffin oil (100) has a value of more than twice as much as the other substances. Also the range of breakage times is higher with paraffin oil (100). The increased viscosity and interfacial tension make the drops of this substance more stable and they are harder to break. One possible explanation of the increased breakage time could be that the paraffin oil (100) drops must remain in the zone of high energy dissipation rate longer in order for breakage to happen, or that they have to get into the region of highest energy dissipation by chance, this region though is quite smaller.

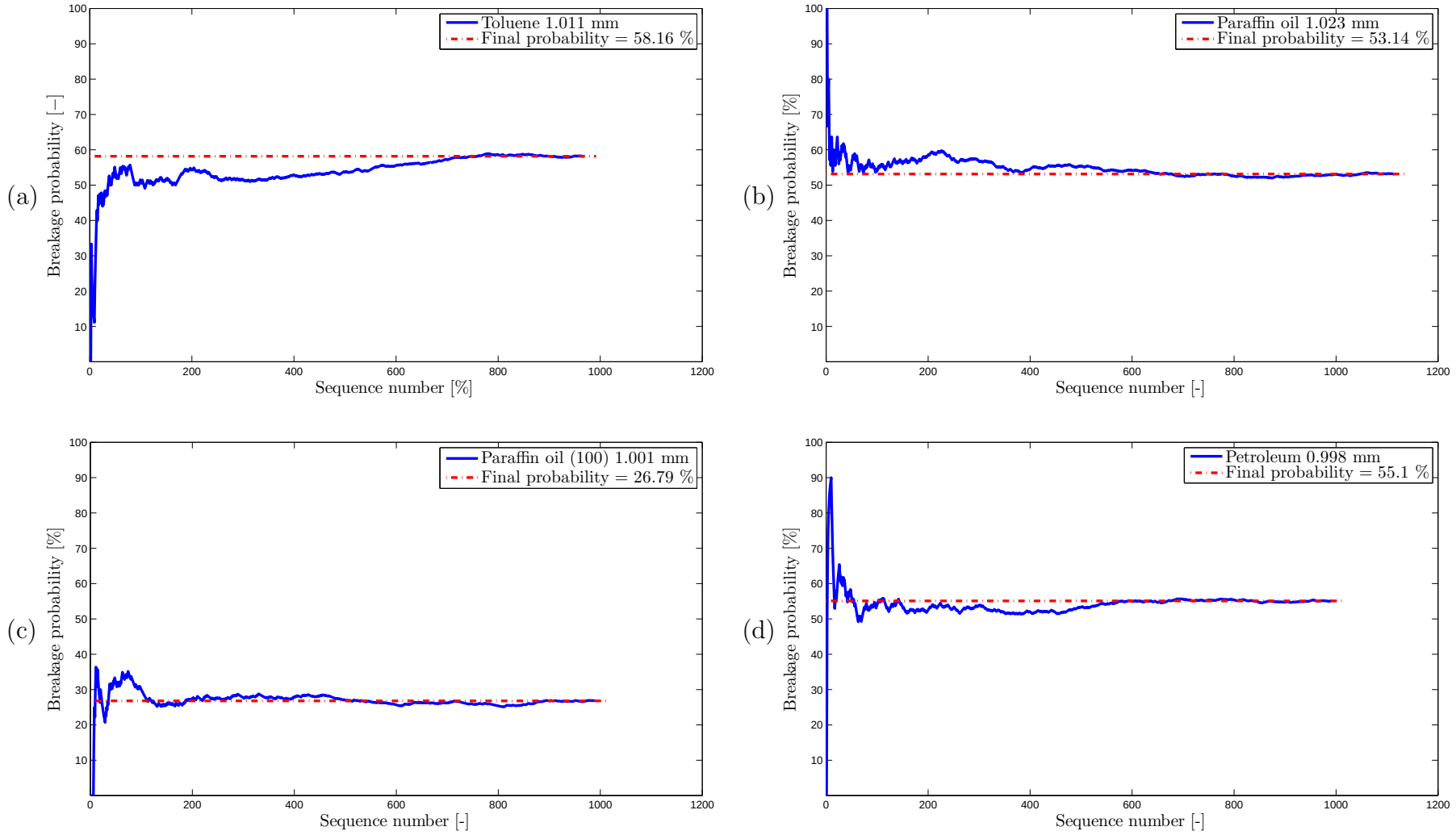

Figure 5.3: Cumulative average breakage probabilities of the 1 mm droplets of (a) toluene, (b) paraffin oil (10), (c) paraffin oil (100) and (d) petroleum

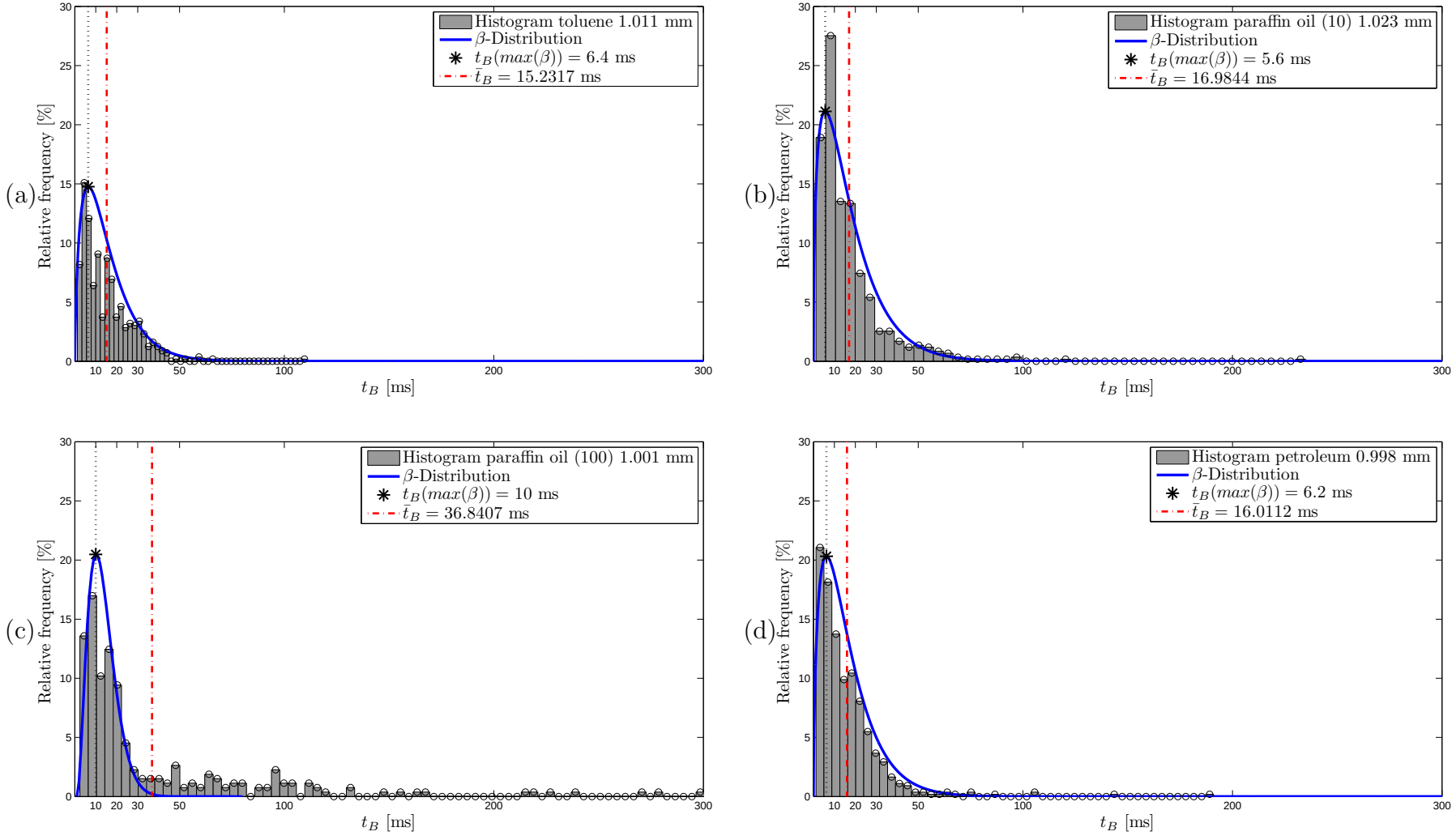

Figure 5.4: Breakage times of the 1 mm droplets of (a) toluene, (b) paraffin oil (10), (c) paraffin oil (100) and (d) petroleum

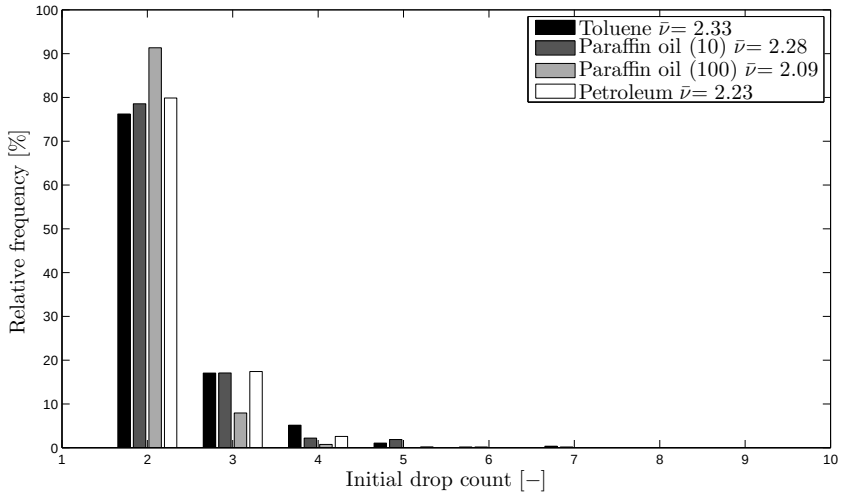

Figure 5.5: Number of initial daughter drops

Initial drop count: The number of drops after the first breakage event was counted and the histogram is shown in Figure 5.5. Binary breakage is by far the most prominent. The average initial number of drops is shown in Table 5.2.

The high viscosity paraffin oil (100) showed once again a different behaviour than the other substances. Its mean number of initial drops is lower than that of toluene, paraffin oil (10) and petroleum, between which no big difference could be observed. The high viscosity oil tends more towards binary breakage. Also its maximum number of initial daughter drops is the lowest of all four substances (toluene: 7 drops, paraffin oil (10): 7 drops, paraffin oil (100): 4 drops, petroleum: 5 drops). A possible explanation could be that the more stable a drop gets the more it tends to show binary breakage. Viscosity and interfacial tension both influence the stability of the drop. When following the trend paraffin oil (10) should be more stable than petroleum and should show more binary breakage. Another possible explanation could be that the time a binary breakage event takes to occur is higher, the more stable a drop gets. Thus being able to detect it as a binary breakage event in the first place. A third possible explanation could be the change of breakage mechanism with a different fraction of binary or tertiary break-ups.

Breakage location: Figure 5.6 shows a visualization of the location of the breakage events on a 2 dimensional grid (exact projected locations). An accumulation of events is visible near the edges of the stirrer blade. This accumulation corresponds to the distribution of the energy dissipation rate as seen in Maaß et al. (2009), yielded by CFD-calculations (Computational Fluid Dynamics). A two-dimensional contour-plot is plotted in Figure 5.7.

Once again the pictures of toluene, petroleum and paraffin oil (10) in Figure 5.6 are comparable. All show a significant fraction of drops breaking in a region near the stirrer blades' edges. The total amount of drops breaking was much lower for paraffin oil (100) but it can be seen that those drops did not break as close to the blade. This can be linked to the behaviour of the breakage time, seen above.

In Figure 5.7 it can be seen that every substance, except for paraffin oil (100), shows a distinct maximum of drop breakage. The high viscosity oil however shows a rather stretched maximum. It might also be noted that paraffin oil (10) as well as toluene and petroleum show another maximum of drop breakage extremely near the stirrer blade edge. The high viscosity oil did not show such behaviour in the experiment. Also no breakage events far away from the stirrer blade could be recorded for the high viscosity oil. This shows that the breakage initiation correlates with the energy dissipation rate.

The breakage events of paraffin oil (100) seem to be distributed in a similar fashion as the other substances except for the extreme positions very near to and far away from the stirrer blade. Drop breakage is not only concentrated in regions of the highest energy dissipation rate, so this assumption (in paragraph: Breakage time) can be dismissed. One explanation could be that breakage takes longer to occur and therefore the drop has moved further away from the spot where breakage started, the spot of the drop-eddy collision (region of high energy dissipation). The fact that no distinct maximum of drop breakage is visible in closest vicinity of the stirrer blade supports this hypothesis. However the drop breakage is not slow enough for the drop to reach a region far away from the stirrer blade and then break.

The low viscosity substances show a maximum short after the stirrer blade, which belongs to the region of the highest energy dissipation rate. They however, also break in the regions far away from the stirrer blade. Being less stable, they might tend to break faster and the distinct maximum near the stirrer blade could be explained. Them being less stable could also explain drop breakage in the lower energy dissipation rate zones far away from the blade. The energy threshold where the drops break is lower with less stable drops than with the high viscosity oil drops. Another explanation for the behaviour of paraffin oil (100) could be that the breakage mechanism changed from drop-eddy collisions to other processes. Observations during the experiment could support this hypothesis.

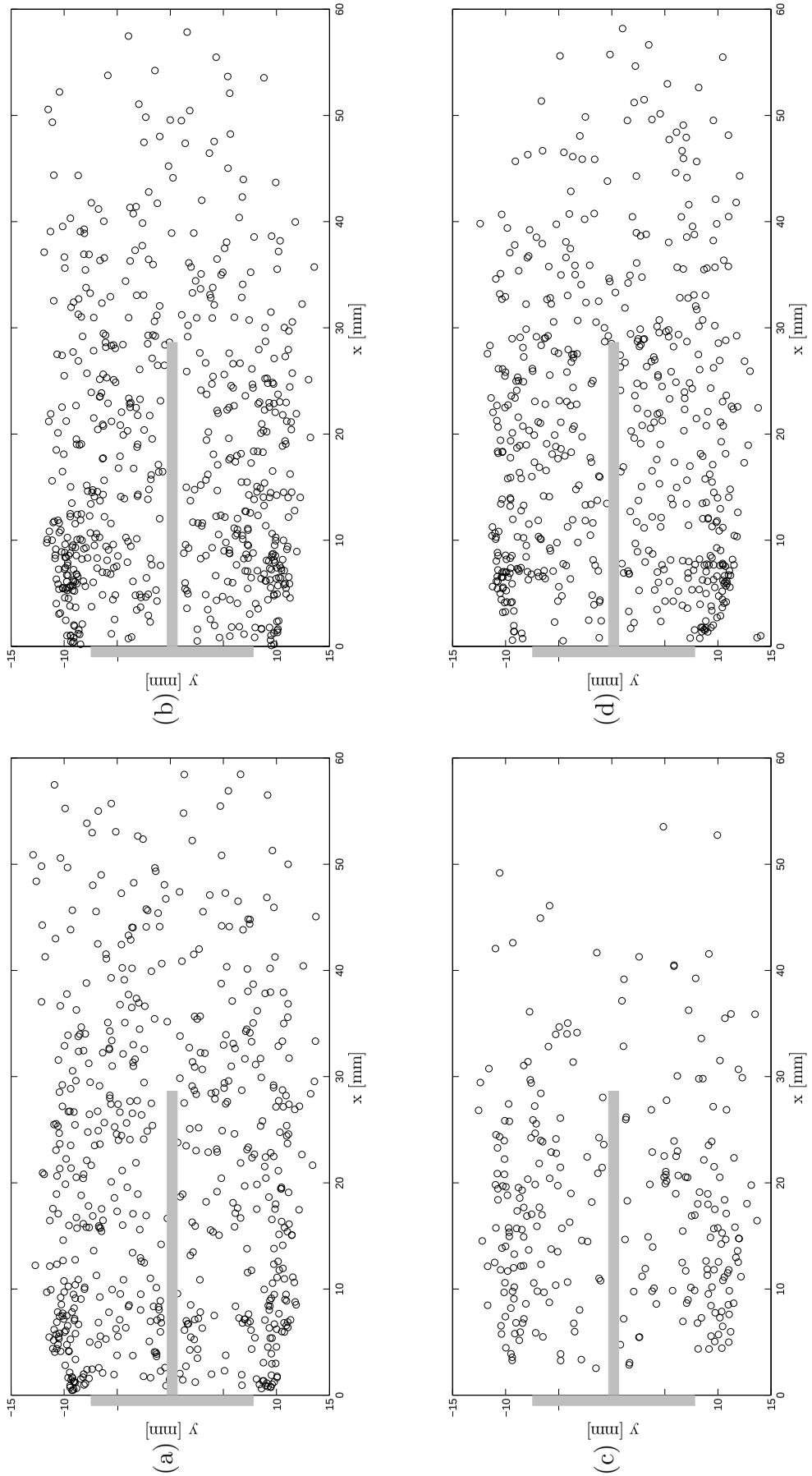

Figure 5.6: Breakage location of the 1 mm droplets of (a) toluene, (b) paraffin oil (10), (c) paraffin oil (100) and (d) petroleum, Part 1

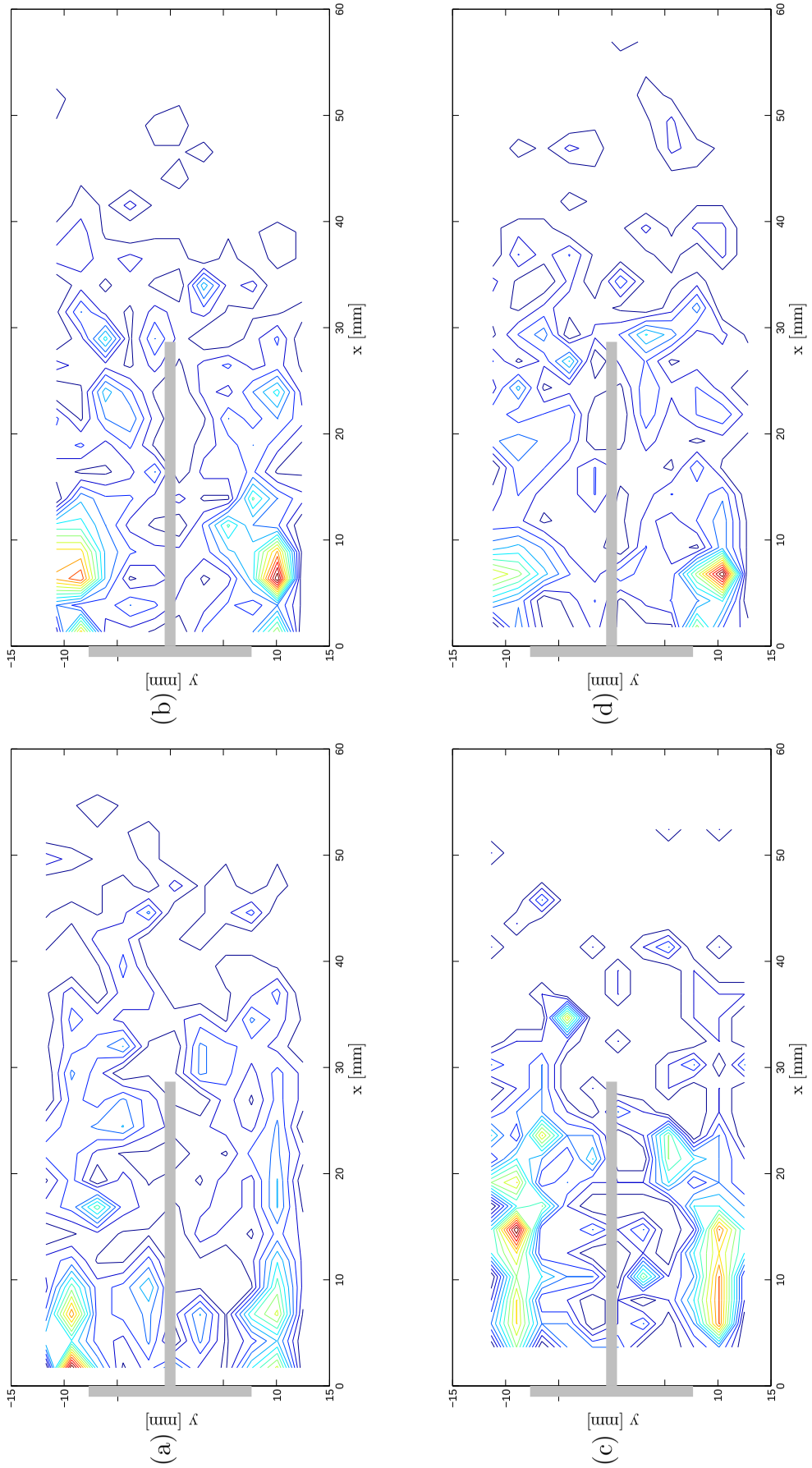

Figure 5.7: Breakage location of the 1 mm droplets of (a) toluene, (b) paraffin oil (10), (c) paraffin oil (100) and (d) petroleum, Part 2

Table 5.2: Summary of experimental data 1 mm

	P [%]	t_B [ms]	$g(d_p)$ [1/s]	$\bar{\nu}$ [−]
Toluene	58.16	6.4	**90.63**	2.33
Paraffin oil (10)	53.14	5.6	**94.64**	2.29
Paraffin oil (100)	26.79	11.4	**23.51**	2.09
Petroleum	55.10	6.2	**88.71**	2.23

Breakage rate: The breakage rates of toluene, petroleum and paraffin oil (10) are close together, only the value of the high viscosity oil is different. With the breakage time being twice as much and the breakage probability being half as much as the values for the other substances, the breakage rate is approximately one quarter of the value of the other three. The exact values can be seen in Table 5.2.

In Figure 5.8 one can see the breakage rates of all four substances plotted over the viscosity of the dispersed phase and over the interfacial tension. It is evident that until a value of 10 mPa s the breakage rate of one diameter is in the same range. The value of 100 mPa s is way off that trend. The preceeding paragraphs showed an influence of the system properties on the values of breakage probability and breakage time, leading to an influence on the breakage rate. The most stable substance tested, paraffin oil (100), has the lowest breakage rate.

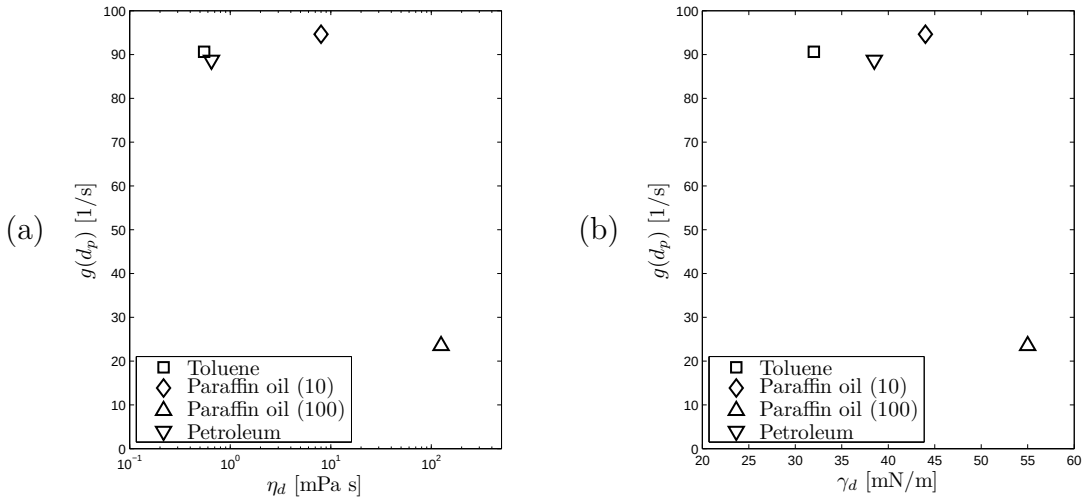

Figure 5.8: Breakage rate for the four substances (diameter 1 mm) over viscosity (a) and interfacial tension (b)

Qualitative predictability by models: This general trend of the breakage rate could be predicted by the model of Alopaeus et al. (2002) that includes viscostiy. The viscosity is in the numerator part of the argument of the complementary error function (erfc). When the argument is increasing, the complemenary error function is decreasing. This is enhanced by the increasing interfacial tension being in the numerator part as well. When only considering the interfacial tension, the model of Coulaloglou and Tavlarides (1977) also could predict a decreasing breakage rate when the interfacial tension increases. This is because interfacial tension multiplied by minus one is in the numerator of the exponent of Euler's number. Martínez-Bazán et al. (1999) shows a similar trend, here the viscosity increasing decreases the value unter a square root. For paraffin oil (100) not having the highest density, the behaviour of the breakage rate can not be explained by density alone.

Comparision with previous data: When comparing the breakage rates calculated here with prior research one gets the diagram in Figure 5.9. One sees three models, fitted by Zillmer (2010), old experimental data (plus signs) and the data of this work. The data points used are toluene at 822 fps. It can be seen that the data point created in this work is in the same general region as the one in prior works, but are not matching exactly. When dividing the breakage rate into its components, breakage probability and breakage time, one can see that the data point of the breakage probability created in this study fits very well to the data point of the previous work. The breakage time however varies more significantly (being more than two times as much). The influence of the experimenter on the breakage probability seems to be insignificant. The influence on the breakage time is more prominent. It leads to a factor of approx. two in the breakage rate. Some more sources of error are laid out in subsection 5.4. Another parameter fitting could be necessary to see the influence on the model choice.

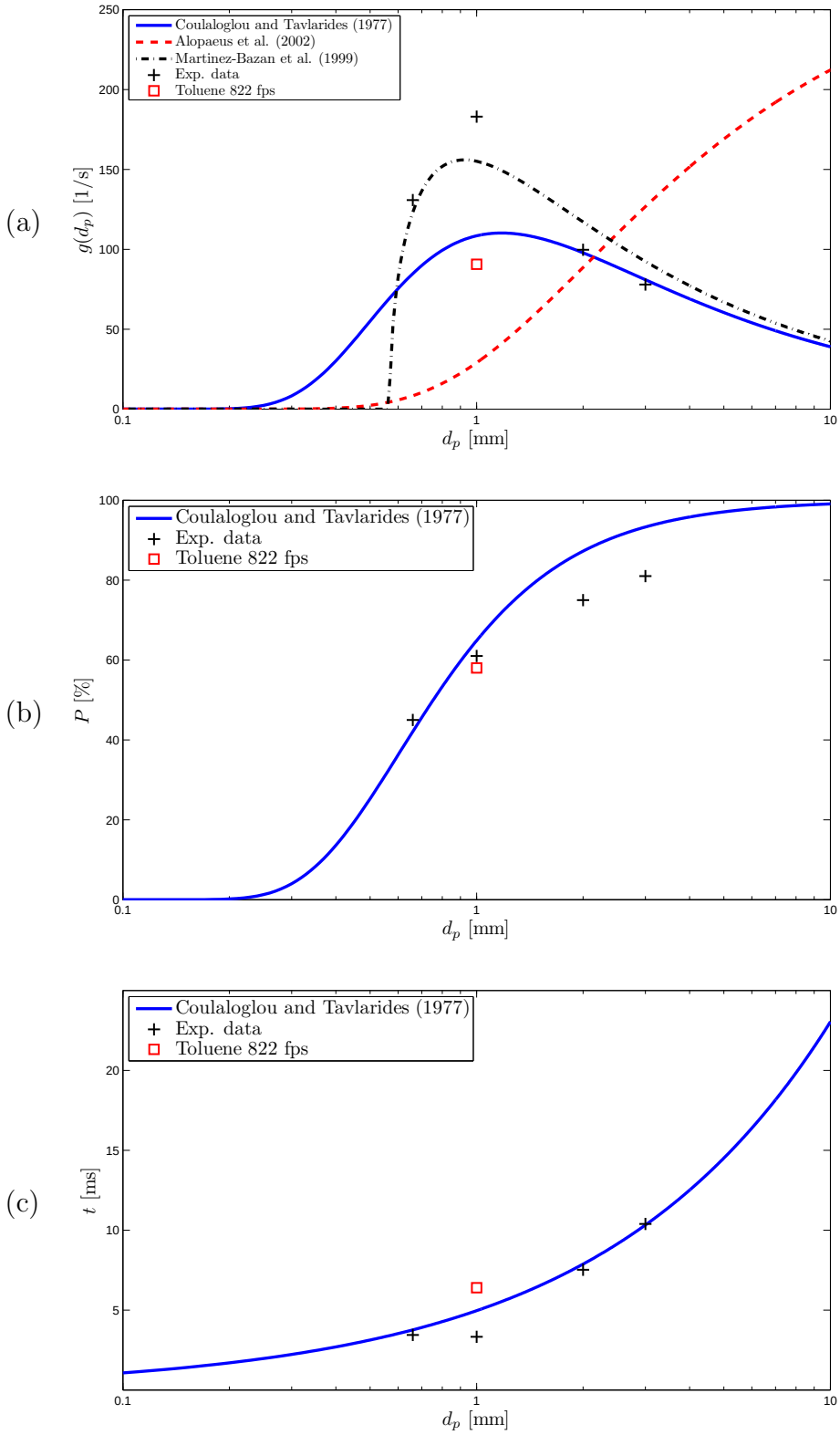

Figure 5.9: Data points in comparison of the breakage rate (a), the breakage probability (b), and the breakage time (c) to earlier work

Table 5.3: Comparison of full and half picture for toluene

	P [%]	t_B [ms]
Full picture (822 fps)	58.16	6.4
Half picture (1450 fps)	53.82	5.1
Half picture (725 fps)	54.24	7.2

5.2 Framerate

When doing breakage experiments, it can be seen, that often more than two initial daughter drops are registered. To investigate the influence of the time resolution on the recognised breakage events the breakage experiment was conducted with another, higher framerate of 1450 fps. For the data rate limitation could not be exceeded, the observed area had to be bisected. The experiments were conducted with toluene and the results of the following sequences was analysed for the influence of the framerate on the initial number of daughter drops:

- Full picture, 822 fps
- Half picture, 1450 fps
- Half picture, 1450 fps (2), same raw data as above but every other picture was deleted to simulate a lower framerate of 725 fps

Comparison of breakage rate and time between full and half picture: In Table 5.3 the breakage rates and breakage times are seen for the full picture (822 fps) and the half pictures (1450 fps and 725* fps). The breakage rate of the full picture experiment is higher than the breakage rates of the half picture experiments. This could be explained by drops changing sides and breaking there, lost to the image bisection. Those drops were not recorded because they could not have been subjected to the automated image processing (see subsection 5.4). The difference between both half picture results could be explained by taking into account the manual setting of the region of interest (see subsection 5.4). The region of interest setting was different in each analysis.

The breakage time shows a similar behaviour when comparing the full picture (822 fps) with the half picture of 1450 fps, the value of the half picture is reduced. The breakage time of drops caught by eddies and transported to the other side could be higher than for those drops remaining on one side. The half picture of 725* fps however shows a higher breakage time than the others. An influence of the framerate could explain this. When reducing the framerate, fast breakage events are no longer distinguishable from slower breakage events and the breakage time increases. The breakage time of the 725* fps analysis is close enough to the value of the full picture and slightly higher to match the trend.

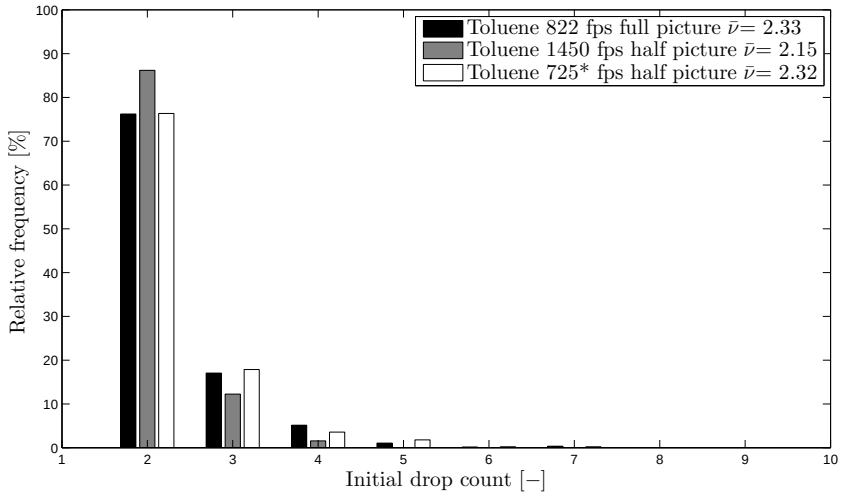

Figure 5.10: Number of initial daughter drops, adjusted framerate

Comparison of the initial numbers of daughter drops: Figure 5.10 shows a composition of three initial numbers of daughter drops. It can be seen that the mean value of the 822 fps is lower than the one of 1450 fps. The distribution of the higher framerate is shifted towards binary breakage. The count for three or more daughter drops is decreasing. As a check every other picture of this high framerate was deleted and the images were once again subjected to the image processing. The resulting values are displayed in the third bar. It is evident that these values are similar to the ones of 822 fps. One possible way to explain this influence is to say that there is only binary breakage but it is only visible with very high framerates. When more than two initial daughter drops are registered, this could mean that one sees the result of a succession of binary drop break-ups.

5.3 Needle type and entry point

In order to create small droplets the glass cannula with the smallest inner and outer diameter was tested with toluene. The motherdrop analysis showed a deviation from the desired diameter that was too high. It is visible that there are two distinct maxima. One possible explanation is to suggest two methods of drop ablation. On the raw unaltered images those two mechanisms can be distinguished. The first is an ejection of the drop out of the glass cannula by impulse of the dosing pump. The other one is debonding without that impulse, only due to the continuous phase fluid flow, leading to larger drops. Due to breaking down after this experiment, no other motherdrop diameters could be tested with this cannula.

Table 5.4: Summary of smallest drops

	d_p [µm]	Needle position	Gauge
Toluene	435	top	33
	321	middle	- (glass)
Paraffin oil (10)	465	top	33
Paraffin oil (100)	357	top	33
Petroleum	286	top	33

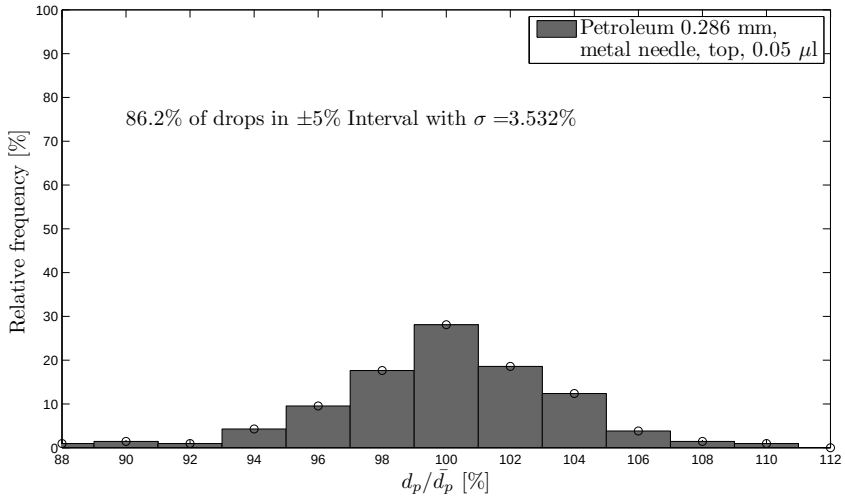

Figure 5.11: Histogram of smallest achievable drop with a metal needle (petroleum)

The smallest overall mother drop generated was with petroleum and a histogram is shown in Figure 5.11. Figure 5.12 shows the histograms of the smallest mother drops for toluene, paraffin oil (10) and paraffin oil (100) that were generated. The value of 0.05 µl is the drop volume selected at the software interface controlling the pump and it corresponds to a drop diameter of 228 µm. It is evident that the drop sizes generated are always bigger than that value. Although standardised and purchasable, the use of metal needles has disadvantages. One major drawback is the adhesion of drops to the metal needle. This effect seemed to be stronger than for the glass cannula. The generation of small drops ($d_p \leq 700$ µm) turned out to be very difficult. Due to interfacial tension between toluene, water and steel the small drops adhere to the front surface of the needle tips. The goal was to minimise that face surface by altering the wall thickness and by purchasing needles with other point styles. The toluene drops created with the glass cannula however were considerably smaller, so this should be used instead of metal. This is also the case for the other substances, though not as prominent. It was not possible to create stable toluene drops smaller than 400 µm with the smallest straight metal needle. To ensure that the drops would not adhere to the metal needle, it was slightly bent upwards, but no smaller drops could be generated.

The entry point was also varied and with it the fluid velocity at the generation position (see Figure 3.2). Observation showed that the higher the fluid velocity, the smaller the drops became, as expected. Another variable is the volume pumped into the needle by the pump. It was observed that this volume did not have a significant effect on the resulting mother drops when using the smalles possible needle. With bigger needles the pressure increase could be harnessed to give the generated drop some kind of impulse. This impulse was weakened by the small inner diameter of the metal needle used. A summary of the smallest drops created during this work can be seen in Table 5.4

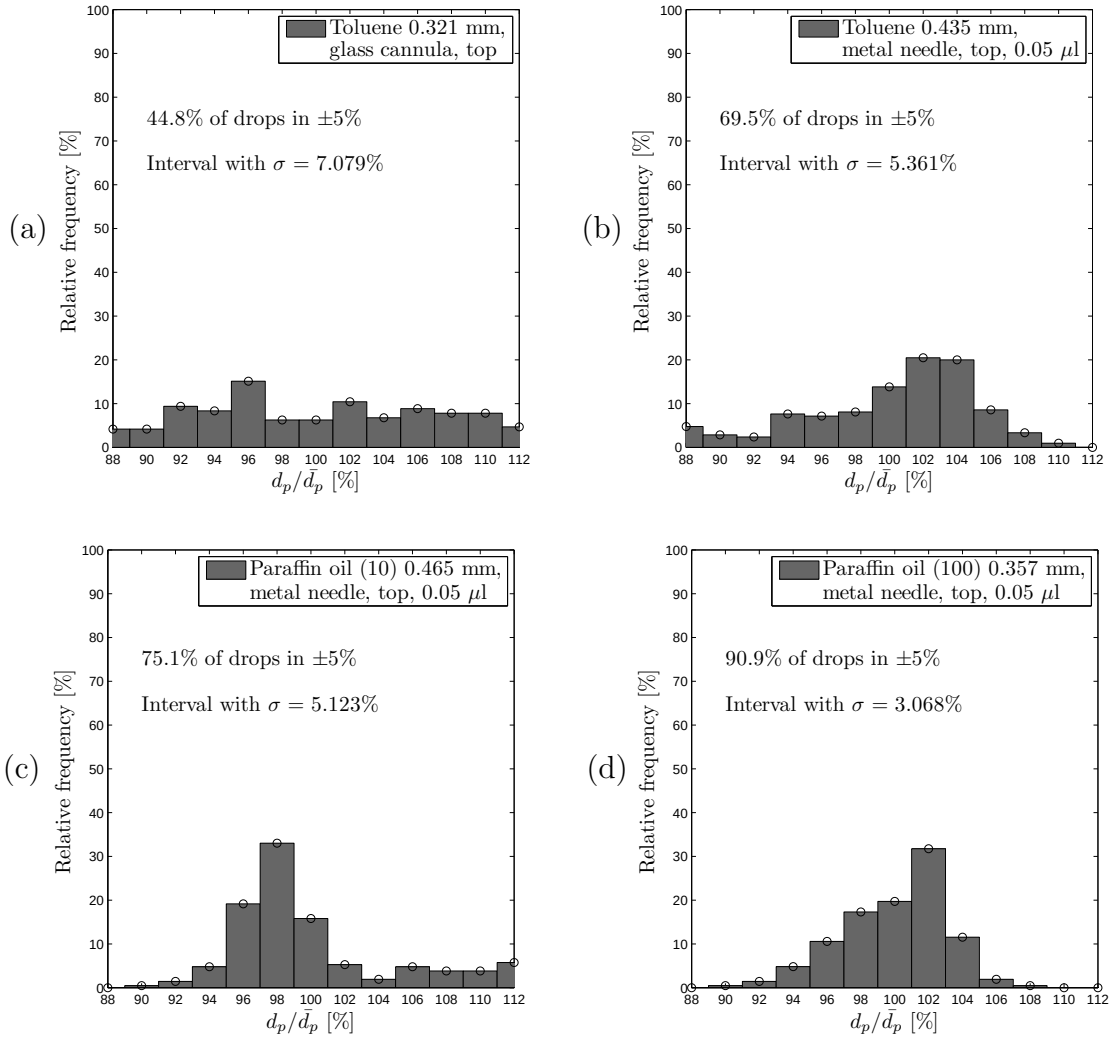

Figure 5.12: Histograms of the smallest droplets of toluene with glass cannula (a), toluene with metal needle (b), paraffin oil (10) with metal needle (c) and paraffin oil (100) with metal needle (d)

5.4 Possible sources of error

The image taking process is highly subjective. The breakage probability clearly depends on how well the experimenter sees the drops moving through the image area. It was seen that breaking drops are more visible than not breaking ones because those do not stay in the image area long enough. Calculations showed that not breaking drops, travelling with the flow at 1.5 m/s only stay in the image area for 0.04 s when they are carried by the fluid flow straight through the channel section. At a framerate of 822 fps this means the drop is only visible on 33 consecutive frames. A monitor however only displayes a small fraction of those 33 frames (about two or three frames) because it has an inherent framerate.

As seen in Section 3.2.2 the image processing uses a simple mass balance to check the drop diameter in the picture. The perspective problem indirectly influences the result of that check, because drops nearer to the camera appear bigger than drops near the back wall. This can lead to false error messages.

Every image processing procedure involves some manual input, be it the drawing of a region of interest, or the definition of the unit length. This unit length has to be measured manually. When analysing the mother drops usually the needle tip is this reference length, when doing the breakage analysis it is the thickness of the blade mounting. This brings in an error in the range of ≈ 0.1 mm when one misses the real dimensions by one pixel (at a resolution of 10 Pixel/mm). This error decreases when using a telecentric lens at a resolution of 100 Pixel/mm , where it is in the range of ≈ 0.01 mm.

Furthermore, if the droplets created by the breakage process are too small, they are not being recognised by the image processing. That was a compromiss between high accuracy and false error messages because of air bubbles in the channel. The flowrate indicated by the meter fluctuated by a value of about ± 5 l/h.

The assumption of a symmetrical entry into the stirrer zone is not entrirely exact, so the results depend on which side is picked for processing (Maaß et al., 2009). The breakage rate, time and initial number of daughter drops might also depend on the path the drop takes through the stirrer zone. When bisecting the image, it was seen that one lost those drops in the image processing that change sides after entering the observed zone. Those drops either break, or they do not. This however might have other breakage probabilities than measured here.

6 Summary and Outlook

In the preceeding section 5 it can be seen that the dispersed phase properties do have an influence on the breakage rate. It is evident that a more stable drop (higher viscosity and interfacial tension) has a decreased breakage rate. Experiments in the future can show how exactly that influence presents itself on drop breakage and it should be tested quantitatively. This should be done by fixing one value and varying the other one. The influence of the dispersed phase properties should be investigated by varying the density, the interfacial tension and the viscosity. It should also be investigated if a change of breakage mechanism really occurs with more stable drops. Furthermore a detailed parameter fitting should be conducted to find either new models or chose one of the existing models, to represent the data. To help with this choice, smaller drops should be analysed in breakage experiments as this could exclude some of the models from the choice. As an example it can be mentioned, that if no minimum drop diameter is found, as predicted by Martínez-Bazán et al. (1999), below which no breakage occurs, this model could be excluded.

It was seen that the number of initial daughter drops decreases with increasing framerate. This substantiates the assumption of binary breakage. This influence of the framerate should be further tested in future experiments. The number of initial daughter drops also depends on the system properties. Experiments with a more different substances could specify this influence and tell which properties are dominant.

Drop generation depends on the system properties, and on the means of drop creation. The smaller the drop gets, the more difficult it is to create. It was evident that glass needles are preferable to metal needles when it comes to the generation of toluene drops. The influence of glass needles on other substances should be investigated further. It is possible to introduce small, industrially made glass needles to overcome the strong adhesion of drops to the metal needle. Smaller, especially produced metal needles could help to create even smaller drops for petroleum and paraffin oil.

When observing breakage events with small drops, the necessary improvements to ensure a high image resolution as seen in section 4 should be made. Especially exceeding the data rate limits promises to be fruitful. It was shown that small drops can indeed be generated using this set-up and need further investigation.

To overcome the influence of the experimenter on the results (breakage time or probability for example) a triggering mechanism could be created to further automate the set-up and to catch every event, breakage or not.

The influence of the above mentioned factors on the daughter drop distribution should also be investigated. In order to get rid of most of the expensive experimental work, a simulation of the events in the breakage channel using a population balance equation solver could be used to generate more results. Those results however should be validated by experiment.

A Listings

References

Alopaeus, V., Koskinen, J., Keskinen, K.I., 1999. Simulation of the population balances for liquid–liquid systems in a nonideal stirred tank. Part 1 Description and qualitative validation of the model. Chemical Engineering Science 54, 5887–5899.

Alopaeus, V., Koskinen, J., Keskinen, K.I., Majander, J., 2002. Simulation of the population balances for liquid–liquid systems in a nonideal stirred tank. Part 2 parameter fitting and the use of the multiblock model for dense dispersions. Chemical Engineering Science 57, 1815–1825.

Andersson, R., Andersson, B., 2006. Modeling the Breakup of Fluid Particles in Turbulent Flows. AIChE Journal 52, 2031–2038.

Bahmanyar, H., Slater, M.J., 1991. Studies of Drop Break-up in Liquit-Liquid Systems in a Rotating Disc Contactor Part I: Conditions of no Mass Transfer. Chemical Engineering & Technology 14, 79–89.

Calabrese, R.V., Chang, T.P.K., Dang, P.T., 1986. Drop Breakup in Turbulent Stirred-Tank Contactors Part I: Effect of Dispersed-Phase Viscosity. AIChE Journal 32, 657–666.

Coulaloglou, C.A., Tavlarides, L.L., 1977. Description of interaction processes in agitated liquid–liquid dispersions. Chemical Engineering Science 32, 1289–1297.

Gäbler, A., Wegener, M., Schlauch, S., Kraume, M., 2005. Transiente Tropfengrößenverteilungen in gerührten Flüssig/flüssig-Dispersionen. Chemie Ingenieur Technik 77, 80–84.

Galinat, S., Masbernat, O., Guiraud, P., Dalmazzone, C., Noïk, C., 2005. Drop break-up in turbulent pipe flow downstram of a restriction. Chemical Engineering Science 60, 6511–6528.

Konno, M., Aoki, M., Saito, S., 1983. Scale effects on breakup process in liquid-liquid agitated tanks. Journal of Chemical Engineering of Japan 16, 312–319.

Kuriyama, M., Ono, M., Tokanai, H., Konno, H., 1995. The Number of Daughter Drops Formed per Breakup of a Highly Viscous Mother-Drop in Turbulent Flow. Journal of Chemical Engineering of Japan 28, 477–479.

Liao, Y., Lucas, D., 2009. A literature review of theoretical models for drop and bubble breakup in turbulent dispersions. Chemical Engineering Science 64, 3389–3406.

Liao, Y., Lucas, D., 2010. A literature review on mechanisms and models for the coalescence process of fluid particles. Chemical Engineering Science 65, 2851–2864.

Maaß, S., 2005. Experimentelle Bestimmung von Tochtertropfenverteilungen durch Zerfall eines Einzeltropfens an einem Rührerblatt. Diplomarbeit. Chair of Chemical and Process Engineering, TU Berlin.

Maaß, S., Hermann, S., Kraume, M., 2010. Determination of breakage rates with single drop experiments, 4th International Conference on Population Balance Modelling, Berlin.

Maaß, S., Wollny, S., Sperling, R., Kraume, M., 2009. Numerical and experimental analysis of particle strain and breakage in turbulent dispersions. Chemical Engineering Research and Design 87, 565–572.

Martínez-Bazán, C., Montañés, J.L., Lascheras, J.C., 1999. On the breakup of an air bubble injected into a fully developed turbulent flow. Part 1. Breakup frequency. Journal of Fluid Mechanics 401, 157–182.

Narsimhan, G., Gupta, J.P., 1979. A model for transitional breakage probability of droplets in agitated lean liquid-liquid dispersions. Chemical Engineering Science 34, 257–265.

Paschedag, A., 2004. CFD in der Verfahrenstechnik - Allgemeine Grundlagen und mehrphasige Anwendungen. Habilitationsschrift. TU Berlin.

Paul, E.L., Atiemo-Obeng, V., Kresta, S.M., 2004. Handbook of industrial mixing: science and practice. John Wiley & Sons, Inc.

Thöniß, T., 2004. Abbildungsfehler und Abbildungsleistung optischer Systeme, Technische Optik in der Praxis, Göttingen (Fachhochschule für angewandte Wissenschaft und Kunst).

Thöniß, T., 2006. Objektive in der industriellen Bildverarbeitung, 2. Fachtagung Optische Industriesensorik, Böblingen.

Zillmer, M., 2010. Bestimmung experimenteller Bruchraten von Toluoltropfen in Wasser anhand von Einzeltropfenuntersuchungen. Diplomarbeit. Chair of Chemical and Process Engineering, TU Berlin.

List of Figures

List of Tables